

Observations of Nitrogen Oxides and Volatile Organic Compounds in the North China Plain and Impact on Ozone Production

Sarah E. Benish

A scholarly paper in partial fulfillment of the requirements for the degree of

Master of Science

May 2019

Department of Atmospheric and Oceanic Science, University of Maryland
College Park, Maryland

Advisor: Dr. Russ Dickerson

Table of Contents

Abstract	1
Acknowledgements	2
List of Tables	3
List of Figures.....	5
List of Abbreviations.....	7
Chapter 1. Introduction	8
Chapter 2. Materials and Methods	15
2.1 Air Sampling and Analysis.....	15
2.2 Estimates of VOC Reactivity.....	23
2.2.1 OH Reactivity	23
2.2.2 Ozone Formation Potential.....	23
2.2.3 Photochemical Ozone Creation Potential (POCP)	24
2.3 Identification of VOC Sources	25
2.4 Box Model Simulations	26
2.4.1 Ozone Production and Sensitivity Calculations	27
Chapter 3. Results	29
3.1 Nitrogen Oxide Observations.....	29
3.2 Volatile Organic Compounds.....	31
3.2.1 Observations	31
3.2.2 Levels and speciation of VOCs	32
3.2.3 OH Reactivity	33
3.2.4 Ozone Formation Potential (OFP).....	35
3.2.5 Photochemical Ozone Creation Potential	37
3.2.5.1 Comparison of OFP and POCP	38
3.3 Photochemical Ozone Production Rate and Sensitivity.....	39
3.4 Comparison to Colorado Front Range experiment: FRAPPÉ.....	41
3.4.1 Nitrogen Oxide Observations	42
3.4.2 Volatile Organic Compounds.....	42
3.5 Major Sources of VOCs.....	47
Chapter 4. Discussion	51
Chapter 5. Conclusions	55
References	57

Abstract

Ground-level ozone (O_3) is becoming increasingly severe in China despite reductions in many precursor emissions. To provide insight into O_3 and its precursors, we report on research flights from the Air chemistry Research In Asia (ARIAs) campaign in spring 2016 based in the North China Plain (NCP). In the planetary boundary layer (PBL) below 500 m, box model calculations constrained by measured precursors indicate the peak rate of O_3 production was ~ 13 ppbv/hour. In the lower free troposphere, frequently polluted with CO (~ 200 ppbv) and NO_2 (~ 100 pptv), O_3 production rates were up to 5 ppbv/hour, conducive to long range transport. Measurement of 74 nonmethane hydrocarbons (NMHCs) and halogenated halocarbons (HHs) reveals alkanes dominated the total volume mixing ratio of volatile organic compounds (VOCs), but alkenes were responsible for 38% of the total VOC reactivity assessed by calculating the OH loss rates. The influence of specific VOC species on O_3 photochemical production was evaluated using ozone formation potential (OFP) and photochemical ozone creation potential (POCP), which suggests aromatics, alkenes/alkynes, alkanes, and the halocarbon vinyl chloride are responsible for the most O_3 formation. ARIAs observations are compared with aircraft measurements over Colorado's Front Range under similar situations such as the location in the midlatitudes and geographic environment. Sources of VOCs in the Front Range include oil and natural gas operations and automobile sources, while in the North China Plain consist of biomass burning, vehicular emissions, and petrochemical processes including oil and natural gas.

Acknowledgements

First, thank you to my advisor Dr. Russell Dickerson for his ongoing support and guidance throughout my academic career at the University of Maryland. I gratefully acknowledge the help of Dr. Tracey Holloway from the University of Wisconsin for encouraging me to apply to graduate school. I would also like to extend my sincere thanks the ARIAs science team, particularly Xinrong Ren and Hao He, for their contributions to the analysis provided here. I am also thankful for the support from the atmospheric chemistry group at the University of Maryland and the support of faculty and staff who I work closely with. Lastly, thank you to my family and friends, as I would not be where I am today without their long term encouragement and support.

List of Tables

<u>Table</u>	<u>Page</u>
Table 2.1: Y-12 Instrumentation during ARIAs.	17
Table 2.2: The NMHCs and HHs measured during ARIAs (median and mean \pm standard deviation (sd), ppbv). The total number of valid samples used in statistics is given in the parentheses.....	20
Table 3.1: Top 15 species ranked by median volume mixing ratio (Unit: ppbv) as well as mass concentration (Unit: $\mu\text{g}/\text{m}^3$) and percentage contribution to total VOC mixing ratio and speciated mixing ratio during ARIAs.	33
Table 3.2: Top 15 species ranked by median OH reactivity (s^{-1}) and percentage contribution to total OH reactivity and speciated OH reactivity during ARIAs.	34
Table 3.3: Top 15 species ranked by median ozone formation potential (ppbv O ₃) using maximum incremental reactivity (MIR) and percentage contribution to total OFP and speciated OFP during ARIAs.	36
Table 3.4: Top 15 species ranked by median POCP-weighted mixing ratio (ppbv) and percentage contribution to total POCP and speciated POCP during ARIAs.....	37
Table 3.5: The top 5 NMHCs measured during FRAPPÉ in Denver ranked by median volume mixing ratio, OH reactivity, OFP, and POCP. The percentage contribution to total and speciated volume mixing ratio, OH reactivity, OFP, and POCP are given in %.	45
Table 3.6: The top 5 NMHCs measured during FRAPPÉ in Weld County ranked by median volume mixing ratio, OH reactivity, OFP, and POCP. The percentage contribution to total and speciated volume mixing ratio, OH reactivity, OFP, and POCP are given in %.	46

Table 3.7: Average CH₄ and enhancement compared to global monthly average for all data, data when benzene/toluene (B/T) >1, and when benzene/toluene < 1 for ARIAs and FRAPPÉ. 51

List of Figures

<u>Figure</u>	<u>Page</u>
Figure 2.1: Left: Average May 2016 OMI tropospheric column NO ₂ from NASA Goddard Earth Sciences Data and Information Services Center. The NCP is clearly seen in the center with high column NO ₂ concentrations; rectangle indicates general area of flights. Right: Map of 11 ARIAs flight tracks (colored lines) and location of VOC samples (black triangles).....	15
Figure 3.1: Altitude profiles of NO (left), NO ₂ (middle), and NO _y (right) averaged every 500 m. The whiskers show the 5th and 95th percentiles; the red box edges show 25th and 75th percentiles and the central black line indicates the median.....	29
Figure 3.2: Median profiles of NO (top), NO ₂ (middle) and NO _y (bottom) at four locations: Julu (red), Quzhou (blue), Shijiazhuang (green), and Xingtai (pink). Grey points are all data and the dashed black lines indicate the 5th and 95th percentiles. All units are ppbv.....	30
Figure 3.3: Left: Net O ₃ production rate calculated using box model results along the Y-12 flight track during ARIAs. The size of the dots is proportional to the production rate of O ₃ . Right: O ₃ production sensitivity indicator, L _N /Q, along the Y-12 flight track during ARIAs. Ozone production is VOC-sensitive when L _N /Q > 0.5 and NO _x -sensitive when L _N /Q < 0.5.....	39
Figure 3.4: Vertical profiles of the O ₃ production rate (left), O ₃ loss rate (middle), and net O ₃ production rate (right) during ARIAs.....	40

Figure 3.5: Median mixing ratios (ppbv) of the top 10 species contributing to total VOC mixing ratio in China (blue). Median values measured during FRAPPÉ in Denver and Weld County are shown in red and yellow..... 43

Figure 3.6: Slope (k) and correlations (r) of (a) acetylene with ethane, (b) isopentane with n-pentane, and (c) o-xylene with m/p-xylene for ARIAs in China (all samples, red circles) and Weld County (blue triangles), and Denver (green crosses)..... 49

List of Abbreviations

ARIAs- Air chemistry Research in Asia

FR- Front Range

FRAPPÉ- Front Range Air Pollution and Photochemistry Experiment

HH- Halogenated hydrocarbon

MIR- Maximum Incremental Reactivity

NCP- North China Plain

NMHC- Nonmethane hydrocarbon

NO_x- Nitrogen Oxides

O₃-Ozone

OFP- Ozone Formation Potential

OH- Hydroxyl radical

OHR- OH Reactivity

OOs- Oxygenated Organics

POCP- Photochemical Ozone Creation Potential

PM- Particulate matter

ppbv-Part per billion per volume

pptv-Part per trillion per volume

SO₂-Sulfur dioxide

VOC- Volatile organic compound

Chapter 1. Introduction

Explosive urbanization and rapid industrialization contributed to high ground-level ozone (O_3) and particulate matter (PM) over the past several decades in the North China Plain (NCP) (Johnson et al., 2006; Ran et al., 2011; Shao et al., 2009; Q. Zhang et al., 2014). While sulfur dioxide (SO_2) pollution has improved over the past decade (He et al., 2012; Krotkov et al., 2016), surface O_3 levels over China have increased in recent years (G. Li et al., 2017; Lu et al., 2018). Rural household energy use for cooking and heating, as well as large-scale burning of winter wheat residues in the NCP, are just some of the many sources responsible for O_3 precursors, such as nitrogen oxides ($NO_x=NO+NO_2$) and volatile organic compounds (VOCs) (Chen et al., 2017; Long et al., 2016; Stavrakou et al., 2016). Ozone is harmful to both the human respiratory system (Jerrett et al., 2009) and to photosynthetic processes by vegetation (Reich & Amundson, 1985), while some VOCs, such as benzene and chloroform, are known to be hemotoxic, carcinogenic, and harm human health (Environmental Protection Agency - Integrated Risk Information System, 2003; Lan, 2004). Quantifying NO_x and VOC pollution is necessary to better understand the photochemistry of O_3 production in the NCP.

Ozone is created through the oxidation of NO by hydroperoxyl radicals (HO_2) and organic peroxy radicals (RO_2), products of carbon monoxide (CO) and VOC oxidation. When one of these precursors is the limiting reactant, the rate of O_3 production is considered VOC- or NO_x - sensitive (Finlayson-Pitts & Pitts, 1999; Sillman et al., 1990). The role of VOCs on O_3 formation depends on the characteristics of the environment, including the main emission sources of primary pollutants. Many studies have concluded O_3 production in urban areas of China is VOC-sensitive in spring, while likely more

NO_x-sensitive in more rural areas (Ran et al., 2011; Xue et al., 2013). Research also shows O₃ production is altitude dependent; in the Beijing-Tianjin-Hebei region, O₃ formation is limited by VOCs near the surface (G. Tang et al., 2012), but more NO_x-sensitive above 1 km over Beijing (P. Chen et al., 2013).

While biogenic VOC emissions are the largest VOC source globally even in urban areas like the southeast US by as much as a factor of 10 compared to anthropogenic sources, emissions from human activities play an important and sometimes determining role in O₃ production (Atkinson & Arey, 2003; Helmig & Bottenheim, 2009; Klimont et al., 2002). Studies in China indicate anthropogenic VOC emissions have increased by 29% by mass from 2001-2006 or at an annual average rate of 7.4% from 22.45 Tg in 2008 to 29.85 Tg in 2012, with Hebei province among the top emitters (R. Wu et al., 2016; Q. Zhang et al., 2009). Gasoline vehicles, biomass burning, industrial processes, and fossil fuel combustion were listed as the top four emission sources in 2005 in Hebei (Bo et al., 2008), and other studies point to industrial VOCs contributing most to O₃ formation in China (Klimont et al., 2002; G. Li et al., 2017; Wei et al., 2008).

Alkanes have been found to contribute over half of the total VOC concentration in late spring in the Beijing-Tianjin-Hebei region, followed by alkenes and aromatics (Cai et al., 2010; L. Li et al., 2015; J. H. Tang et al., 2009; Yuan et al., 2013). Cai et al. (2010) found measured alcohols, esters, and ethers accounted for 10.6% of the total VOC concentrations in Shanghai throughout all seasons. Y. Liu et al. (2009) found C₂-C₅ alkenes, isoprene, and C₁-C₃ aldehydes were key reactive species in Beijing in August 2005. Despite differences in measurement capabilities throughout studies, ethane,

propane, and acetylene were commonly the most abundant species (Jia et al., 2016; L. Li et al., 2015; Mo et al., 2015; J. H. Tang et al., 2009).

Photochemical mechanisms of VOCs have been studied since the 1980s, but the investigation of reaction rates and pathways is ongoing given the enormous number of VOCs emitted into the atmosphere (e.g. Atkinson & Arey, 2003; Mazzuca et al., 2016). Oxidation of VOCs can lead to nitric acid which effectively terminates O₃ production (Carter et al., 1994) and to alkyl nitrates. Alkene oxidation forms more reactive compounds such as aldehydes and peroxyacyl nitrates that propagate O₃ formation. The calculation of the first-order loss rate of hydroxyl with different VOCs, termed OH reactivity, provides a measure of the potential in an air parcel to produce organic peroxy radicals, the key intermediate species in the production of O₃ (Stroud et al., 2008). OH reactivity has been measured directly throughout China, with NO_x and CO responsible for most of the OH reactivity, followed by VOCs (Fuchs et al., 2017; Kim et al., 2016; Sadanaga et al., 2005). With NO_x and CO responsible for most of the OH reactivity, Li et al. (2015) calculated the OH loss rates of VOCs in the Beijing-Tianjin-Hebei region and found alkenes contributed 50-70% to total OH reactivity of VOCs.

Several approaches have been used to provide insight into successful O₃ mitigation strategies, such as ozone formation potential (OFP) and photochemical ozone creation potential (POCP) (Carter, 1994; Derwent et al., 1996). OFP is calculated using a maximum incremental reactivity (MIR) scale, defined as the amount of O₃ formed from the addition of a small amount of VOC under high NO_x conditions. Aromatics and alkenes have the highest MIR values, reflecting the high potential for these VOCs to form more O₃ than less reactive compounds. Studies in China reported aromatics and alkenes

are the largest contributors to OFP (Cai et al., 2010; Cheng et al., 2010; Jia et al., 2016; Liang et al., 2017; B. Wang et al., 2010; G. Wang et al., 2016; Xie et al., 2008; Zheng et al., 2009). In Shanghai in 2009, aromatics were estimated to contribute 57% to total OFP (Cai et al., 2010). Tang et al. (2007) concluded ethylene, toluene, and m/p-xylene were the main contributors to OFP during spring in the Pearl River Delta (PRD); however, at a remote site, isoprene from biogenic sources contributed large amounts to OFP (J. H. Tang et al., 2007). Liang et al. (2017) developed an industrial VOC emission inventory for 2010 in China and found oxygenated organic compounds account for 17% of the total emission by mass, but comprise only 6.6% of the total OFP.

The POCP is simulated using a photochemical trajectory model under certain atmospheric conditions and standardized relative to the ozone produced per unit mass of ethylene (Derwent et al., 1996). Contrary to the MIR scale, the POCP scale estimates alkylbenzenes are the greatest contributors to O₃ production, with toluene and xylenes the largest contributing VOCs in China (W. Wu et al., 2017). While most studies using POCP have investigated European cities, limited studies in Asia indicate a small number of VOC species, particularly isoprene, ethylene, m-xylene, and toluene, are the largest contributors to regional O₃ formation in the Pearl River Delta (Cheng et al., 2010).

Past observational studies in China observed high concentrations of trace gases such as O₃ and CO within the boundary layer (P. Chen et al., 2013; Dickerson et al., 2007; Ding et al., 2008; C. Li et al., 2010; F. Zhang et al., 2011). Dickerson et al. (2007) found the prefrontal maximum of CO within 1000 m to be ~900 ppb in 2005 in Liaoning Province in northeast China, and Chen et al. (2013) reported ~110 ppbv O₃ within 1000 m in May over the NCP. Large median fluctuations of CO of 126 ppbv were observed in

a remote site in western China due to advection from the northwest where industrial activities and crop burning are prevalent (F. Zhang et al., 2011). Autumn flights in the Yangtze River Delta in 2007 documented large variability in NO_x concentrations, ranging from 3 to 40 ppbv (Geng et al., 2009), while flights over the Yellow Sea in April 2010 found 2.45 ± 1.33 ppbv NO_x (X. Yang et al., 2016), lower than found in previous studies.

Several VOC correlations and ratios can be used to characterize different air pollution sources (Barletta et al., 2005; Jia et al., 2016; G. Wang et al., 2016; Y. Yang et al., 2016). High amounts of acetylene, ethylene, and light alkanes such as propane are likely attributable to exhaust of gasoline vehicles and evaporation of liquefied petroleum gas (Y. Liu et al., 2008). Isopentane is a marker of gasoline evaporation (with small amounts emitted during combustion processes), while CO is a product of incomplete combustion and VOC oxidation or photolysis (Barletta et al., 2005). A ratio of isopentane to n-pentane less than 1 is indicative of oil and natural gas operations, whereas a ratio around 2 is suggestive of vehicular sources. Vehicular emissions are an important source of aromatics and some anthropogenic isoprene (Borbon et al., 2001). A benzene/toluene (B/T) ratio of ~0.5 has been attributed to vehicular emissions, while higher ratios are indicators of biofuel, coal, and biomass burning (Barletta et al., 2005; Brocco et al., 1997; Perry & Gee, 1995). High benzene not correlated with vehicle combustion tracers has been observed in areas of heavy petrochemical industry, such as Houston, TX (Gilman et al., 2009). Previous work has found a higher mean CH₄ concentrations (> 2 ppmv) for Chinese cities with B/T > 1, suggestive of natural gas leakage (Barletta et al., 2005).

The National Center for Atmospheric Research's (NCAR) Front Range Air Pollution and Photochemistry Experiment (FRAPPÉ) collected meteorological and trace gas

measurements, including VOCs, in Colorado's Front Range (FR) in July and August 2014 on board the National Science Foundation (NSF)/NCAR C-130 aircraft. Previous work has documented the major findings of FRAPPÉ and the concurrent NASA campaign, Deriving Information on Surface Conditions from Column and Vertically Resolved Observations Relevant to Air Quality (DISCOVER-AQ) (Pfister et al., 2017). The NCP is suitable for comparison against Colorado's FR due to same situation in the midlatitudes, similar position along geographic features, like flying on the east side of mountains with arid vegetation, and existence of oil and natural gas operations. Oil and natural gas activities are estimated to account for ~50% of the VOC FR emissions (Pfister et al., 2017) and contribute, on average, ~18% (~ 3 ppbv) to photochemical O₃ produced in the FR or 30-40% of the total O₃ production on high O₃ days (McDuffie et al., 2016; Pfister et al., 2017). At the surface, oil and natural gas related VOCs were also found to be the largest contributor to OH reactivity (Abeleira et al., 2017).

Through Chinese/American partnerships with Peking University, Beijing Normal University and the University of Maryland, we conducted a field campaign in Hebei Province, China in Spring 2016 called Air chemistry Research In Asia (ARIAs). We assessed O₃ production from NO_x measured onboard the Y-12 research aircraft and 74 VOC compounds measured from 27 whole air samples (WAS) collected from the aircraft in May and June 2016. The Ministry of Environmental Protection of the People's Republic of China reported that of the top ten cities with the worst air quality in 2016, six of them are located in Hebei, including the capital city of Shijiazhuang. Additionally, the NASA Korea-United States Air Quality Study (KORUS-AQ) occurred around the same time as ARIAs, providing the opportunity to characterize air quality upwind of South

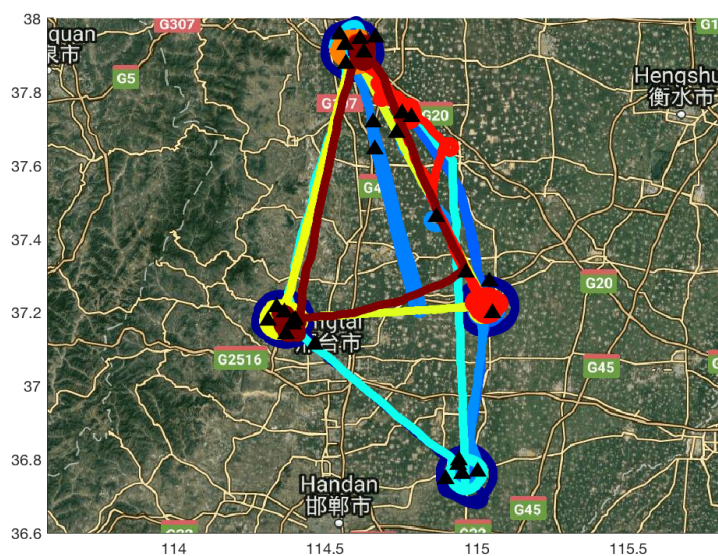
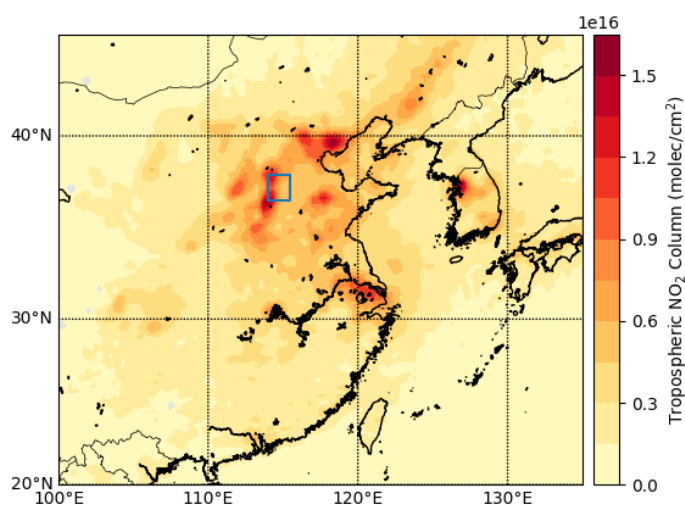
Korea. One objective of this study was to determine what VOC compounds should be targeted to successfully reduce O₃ formation in spring in the NCP. Additionally, we determined the source characteristics of the VOCs to understand what emission sector needs the most reductions in both the NCP and FR.

Chapter 2. Materials and Methods

2.1 Air Sampling and Analysis

The ARIAs campaign in Hebei Province included 11 research flights in May and June 2016 (Figure 2.1). Surrounded by the Taihang Mountains to the west, Yanshan Mountains to the north, and the Bohai Sea and Yellow Sea to the east, the NCP is the largest agricultural plain in China, composing approximately 39% of the arable land (Gao et al., 2014). The Y-12 aircraft was based at Luancheng Airport (114.59°E, 37.91°N, 58 m above sea level (ASL)), located in southeast Shijiazhuang. The Y-12 flew vertical spirals from ~300m to ~3500 m over Shijiazhuang and in three locations: Julu (115.02°E, 37.22°N, 30 m ASL), Quzhou (114.96°E, 36.76°N, 40 m ASL), and Xingtai (114.36°E, 37.18°N, 182 m ASL), all located east of the Taihang Mountains with Xingtai at the foothill (Figure 2.1).

Figure 2.1: Left: Average May 2016 OMI tropospheric column NO₂ from NASA Goddard Earth Sciences Data and Information Services Center. The NCP is clearly seen in the center with high column NO₂ concentrations; rectangle indicates general area of flights. Right: Map of 11 ARIAs flight tracks (colored lines) and location of VOC samples (black triangles).



The Y-12 collected trace gas, aerosol, and meteorology data. The aircraft instrumentation (Table 2.1), included different gas and particle sample inlets on the top of the fuselage and pressure/temperature/humidity sensors (Cloud Water Inertial Probe (CWIP), Rain Dynamics), installed under one wing of the aircraft (Figure S1). Flight position data were recorded using a portable global positioning system (GPS) and the CWIP. The aircraft was equipped with the following trace gas sensors: (1) a Picarro cavity ring down spectrometer (CRDS) for CH₄, CO₂, CO, and H₂O measurements; (2) a Thermal Electron Model 49C UV absorption O₃ analyzer; (3) a Thermal Electron Model 43C pulsed fluorescence SO₂ analyzer; and (4) a Los Gatos Research Model RMT-200 CRDS NO₂ analyzer and a Thermal Environment Model 42C NO-NO_y analyzer. Power constraints and a converter issue led to limited NO_y and NO_x measurements during the campaign. The aircraft was also equipped with an inlet to measure aerosols up to ~5.0 μm diameter and aerosol optical properties, including a nephelometer (TSI Model 3563) to measure aerosol scattering, a particle soot absorption photometer (PSAP) to measure aerosol absorption, and an aethalometer (Magee Model AE31) to measure black carbon. Observed aerosol optical properties have been summarized elsewhere (F. Wang et al., 2018), as well as further details on aircraft instrumentation (Ren et al., 2018).

All 27 whole air samples (WAS) were collected directly into 3.2 L fused silica lined electropolished stainless steel canisters (Entech Instrument Inc., Simi Valley, CA). The WAS cans were cleaned following a standard sampling procedure, pressured with nitrogen and vacuumed three times to 2.6 Pa. The WAS were analyzed by the College of Environmental Sciences and Engineering at Peking University in Beijing with a gas chromatograph equipped with a mass selective detector (GC-MSD, Hewlett Packard

5975/7890, USA) and a flame ionization detector (FID) with a cryofocusing pre-concentration system (Entech Instrument 7100A, Simi Valley, CA) at a constant rate using a mass flow controller.

Table 2.1: Y-12 Instrumentation during ARIAs.

Variable	Method
Aircraft Position	Global Positioning System (GPS)
Meteorology (Temperature, Relative humidity, Pressure, 2-D Wind)	Cloud water inertial probe (CWIP)
Greenhouse Gases (CO ₂ /CH ₄ /CO/H ₂ O)	Cavity Ring Down Spectroscopy Picarro Model G2401-m
Ozone (O ₃)	UV-absorption, TECO 49C
Sulfur dioxide (SO ₂)	Pulsed fluorescence, TECO 43C
Nitrogen dioxide (NO ₂)	Cavity enhanced absorption spectroscopy, Los Gatos RMT-200 CRDS
NO/NO _y	Chemiluminescence, modified TECO 42C External Molybdenum converter at 375°C
Aerosol Scattering, b _{scat} (450, 500, 700, nm)	Nephelometer, TSI Model 3563
Aerosol Absorption, b _{abs} (565 nm)	Particle Soot Absorption Photometer (PSAP)
Black Carbon (370, 470, 520, 590, 660, 880, 950 nm)	Aethalometer, Magee Model AE31
VOCs	Grab Canisters, GC-MSD/FID

A 500-mL aliquot of air sample from each canister was concentrated using a three-stage cryofocusing pre-concentration system. Ambient H₂O and CO₂ were removed in the first two cryotrap using glass beads and Tenax-TA adsorbents, respectively. VOCs were then trapped at -180 °C in the final stage and the trap was rapidly heated, after which VOCs were transferred into the GC-MS/FID system for analysis. This system used a Dean Switch™ (Agilent Technologies, Santa Clara, CA, USA) to introduce the effluent into a DB-624 column (60 m × 0.25 mm × 1.8 μm; J&W Scientific, Folsom, CA, USA) with an MSD to separate and analyze C₄-C₁₂ hydrocarbons and halocarbons. A PLOT (A1/KCl) column (30 m × 0.25 mm × 3.0 μm; J&W Scientific) with an FID to measure the C₂-C₄ hydrocarbons. The GC oven temperature was programmed initially at

30 °C for 7 min, increasing to 120 °C at 5 °C/min and holding for 5 min, and then increasing to 180 °C and holding for 7 min. The entire process took about 47 min. The carrier gas was pure helium (purity > 99.999%).

During the analysis process, strict protocols for quality control and quality assurance were used. The standard gas including Photochemical Assessment Monitoring Stations (PAMS) standard mixture (55 NMHCs) and Toxics Organic-15 (TO-15) standard mixture (65 compounds, from Spectra Gases Inc., NJ, USA) was used to calibrate the C₂–C₁₂ VOCs. Four VOCs with known concentrations, including bromochloromethane, 1,4-difluorobenzene, chlorobenzene-d₅ and 1-bromo-3-fluorobenzene, were used as internal standards for each sample to calibrate the system. The GC-MSD/FID system was calibrated at five concentrations from 0.5 to 8 ppbv for each compound before sample analysis. Correlation coefficients, ranging from 0.987 to 0.999 showed integral areas of peaks were proportional to concentrations of target compounds. The precision of each species was within 5%. A gas standard (diluting from 1 ppm to 2 ppb) was measured each day to check the stability of the system. The method detection limit (MDL) was determined using two methods. The first method is the TO-15 method (Environmental Protection Agency, 1999), where seven replicates are made of the compound of interest near the expected detection limit. The standard deviation is computed from the seven replicates and multiplied by the Student's t value for 99% confidence. The second method is 10 times the instrument noise signal. Since the MS is in selected ion monitoring (SIM) mode, the noise is low. The detection limits (uncertainty ranging from 5-15%) for various compounds ranged from 2 to 50 pptv. Total uncertainty for NMHC and HH measurements reflects instrument noise, plus uncertainty in

calibration standards, line losses, contamination, and pressurization. Best estimate of the total uncertainty is $\pm 20\%$ with 95% confidence due to uncertainties associated with airborne sampling platforms. More details of the VOC analytical techniques have been given elsewhere (Mo et al., 2015; B. Wang et al., 2010).

The sampling periods were approximately 1-2 minutes during the spirals. Since samples were collected at a variety of altitudes from 400 m to 3500 m from the research aircraft between 1:30 and 9:00 UTC (9:30 and 17:00 local time), the data is representative of regional background level VOC mixing ratios and less sensitive than surface-based measurements influenced by nearby point-sources, such as roads and petrochemical facilities. Flight days were selected based on a high probability of an O₃ event and flight tracks did not intentionally sample industry plumes. Thus, the 27 samples in the middle of the boundary layer are representative of the impact of VOCs on O₃ formation and provide guidance into successful control measures. However, one sample collected over Quzhou at approximately 400 m altitude documented a heavily polluted air parcel with little dilution. We leave in this high sample because these measurements are only representative concentrations of this region and affect the mean but not percentile calculations. This sample will be referred to as the anomalous sample throughout this paper.

We also excluded one WAS from this analysis due to evidence of contamination after sampling. This sample was filled to ambient pressure at 3000 m in relatively clean air (CO=111 ppbv, CH₄=1890 ppbv, CO₂=406 ppmv, O₃=84 ppbv), while VOCs for the sample are outliers relative to the trace gases. This is indicative of valve leakage during transit or ambient air entering the WAS can after the flight. The observed acetylene to

CO ratio, often used as a tracer for the age of an air mass, was approximately 70 ppbv/ppbv for the outlier, but much larger (~400 ppbv/ppbv) for samples collected at a similar altitude. Therefore we believe this was the only contaminated WAS.

Table 2.2 summarizes the full list of the 74 VOC species that were identified and quantified, along with median, mean, and number of samples the statistics are based on. VOC species were removed if the number of samples below the detection limit was greater than half of the total number of samples. Species removed include cis-2-pentene, trans-2-pentene, bromodichloromethane, 1,1-dichloroethylene, trans-1,3-dichloropropene, 1,2-dichlorobenzene, 1,3-dichlorobenzene, and 1,2-dibromoethane. We report three significant figures or to 10 pptv to avoid numerical diffusion. A separate paper will further discuss halocarbon, including chlorofluorocarbons, observations.

Table 2.2: The NMHCs and HHs measured during ARIAs (median and mean \pm standard deviation (sd), ppbv). The total number of valid samples used in statistics is given in the parentheses.

Alkanes (27)	Median	Mean \pm sd		Median	Mean \pm sd		Median	Mean \pm sd
Ethane (27)	2553.0	2689.4 \pm 727.4	Propane (27)	1382.0	1445.8 \pm 254.7	n-Butane (27)	35.0	65.7 \pm 60.2
2,2-Dimethylbutane (22)	9.0	33.9 \pm 85.1	2,3-Dimethylbutane (26)	15.0	211.5 \pm 835.1	Isobutane (27)	263.0	1620.4 \pm 5126.3
n-Pentane (27)	77.0	270.1 \pm 765.8	Isopentane (27)	190.0	2896.2 \pm 11433.9	Cyclopentane (22)	19.5	170.5 \pm 603.7
Methylcyclopentane (23)	22.0	69.7 \pm 187.4	2-Methylpentane (27)	72.0	344.6 \pm 1187.6	3-Methylpentane (25)	27.0	202.0 \pm 728.1
2,3-Dimethylpentane (26)	22.5	74.3 \pm 234.9	2,4-Dimethylpentane (26)	11.5	129.3 \pm 493.9	2,2,4-Trimethylpentane (27)	62.0	1157.6 \pm 3999.8
2,3,4-Trimethylpentane (27)	38.0	583.8 \pm 1913.5	n-Hexane (27)	48.0	308.3 \pm 951.9	Cyclohexane (24)	12.5	24.0 \pm 39.2
Methylcyclohexane (26)	11.0	31.5 \pm 70.8	2-Methylhexane (27)	18.0	144.1 \pm 551.5	3-Methylhexane (27)	16.0	161.3 \pm 626.5

n-Heptane (27)	28.0	122.6 ± 419.2	2-Methylheptane (27)	64.0	992.4 ± 3257.8	3-Methylheptane (27)	10.0	31.0 ± 83.8
Octane (27)	21.0	45.9 ± 104.3	n-Nonane (27)	17.0	25.3 ± 21.7	n-Decane (27)	43.0	67.0 ± 63.0
Alkenes/Alkynes (9)	Median	Mean ± sd		Median	Mean ± sd		Median	Mean ± sd
Acetylene (27)	666.0	981.7 ± 745.2	Ethylene (27)	435.0	921.7 ± 930.0	Propylene (27)	457.0	465.3 ± 88.9
1-Butene (27)	259.0	783.9 ± 2231.9	cis-2-Butene (27)	5.0	7.3 ± 7.0	trans-2-Butene (22)	3.0	4.8 ± 3.8
Isoprene (26)	21.5	36.9 ± 39.5	1-Pentene (27)	8.0	9.2 ± 4.7	1-Hexene (18)	7.0	46.2 ± 161.3
Aromatics (16)	Median	Mean ± sd		Median	Mean ± sd		Median	Mean ± sd
Benzene (27)	345.0	528.2 ± 521.4	Toluene (27)	302.0	2252.9 ± 7842.0	Styrene (27)	9.0	24.1 ± 50.7
m/p-Xylene (27)	64.0	316.7 ± 1090.5	o-Xylene (27)	29.0	112.3 ± 356.7	Ethylbenzene (27)	48.0	186.4 ± 595.3
Isopropylbenzene (27)	13.0	17.6 ± 16.2	n-Propylbenzene (27)	10.0	15.6 ± 20.0	2-Ethyltoluene (27)	9.0	14.6 ± 17.4
3-Ethyltoluene (27)	13.0	18.8 ± 18.6	4-Ethyltoluene (27)	11.0	19.2 ± 26.7	1,3-Diethylbenzene (26)	7.5	20.2 ± 48.7
1,4-Diethylbenzene (27)	17.0	25.7 ± 40.7	1,2,3-Trimethylbenzene (27)	13.0	18.1 ± 24.5	1,2,4-Trimethylbenzene (27)	23.0	31.1 ± 31.2
1,3,5-Trimethylbenzene (27)	6.0	10.3 ± 10.9						
Halocarbons (22)	Median	Mean ± sd		Median	Mean ± sd		Median	Mean ± sd
Carbon tetrachloride (27)	89.0	89.1 ± 20.2	Chloroform (27)	74.0	102.6 ± 76.8	Chloromethane (27)	1031.0	1075.0 ± 321.4
Bromomethane (27)	11.0	11.5 ± 2.9	Chloroethane (27)	28.0	42.0 ± 36.1	CFC-11 (27)	283.0	371.3 ± 404.2
CFC-12 (27)	563.0	583.0 ± 111.2	HCFC-22 (27)	368.0	420.7 ± 164.5	CFC-113 (27)	82.0	80.8 ± 3.2
CFC-114 (27)	22.0	42.4 ± 102.1	1,1-Dichloroethane (14)	4.5	17.6 ± 37.1	1,2-Dichloroethane (27)	91.0	122.6 ± 87.5
Cis-1,2-Dichloroethylene (26)	90.5	98.6 ± 78.1	1,1,1-Trichloroethane (27)	2.0	2.5 ± 0.6	1,1,2-Trichloroethane (23)	5.0	10.4 ± 13.6
Trichloroethylene (19)	5.0	5.8 ± 3.1	Tetrachloroethylene (27)	10.0	12.6 ± 7.3	1,1,2,2-Tetrachloroethane (20)	89.0	74.8 ± 44.4

Vinyl chloride (27)	1197.0	1283.2 ± 513.7	1,2- Dichloropropane (27)	83.0	113.4 ± 143.1	Chlorobenzene (26)	6.0	7.9 ± 5.3
1,4- Dichlorobenzene (23)	9.0	13.0 ± 12.9						

Forty eight hour Hybrid Single Particle Lagrangian Integrated Trajectory Model (HYSPLIT) back trajectories were run from the time and location of each WAS, driven by 12 km WRF simulations (He et al., 2019). The trajectories were grouped into distinctive flow patterns: a cold and dry continental polar (cP) airmass entering the NCP or a wet and warm maritime tropical (mT) airmass passing over a heavily industrialized coastal region to the NCP. Fifteen samples were identified as having a cP origin and 12 samples were identified to have a mT origin, all at a variety of altitudes. While meteorology plays an important factor in the airmasses sampled, we aimed to characterize the VOCs measured throughout the campaign. Since a comparable number of samples were found to have cP or mT origins, we conclude these measurements capture a representative background of boundary layer VOCs in spring in the NCP.

The Atmosphere-Aerosol-Boundary Layer-Cloud (A²BC) Interaction Joint Experiment campaign collected meteorological, aerosol, and trace gas information in Xingtai from May to December 2016 (H. L. Wang et al., 2012; Yang Wang et al., 2018; Yuying Wang et al., 2018). An intensive observation period in May and June 2016 was conducted during ARIAs. Data used in this analysis include (1) a NO_x analyzer with a molybdenum converter (Ecotech model 9841A); (2) an infrared absorption CO analyzer (Ecotech model 9830A); and (3) a UV absorption O₃ analyzer (Ecotech model 9810A). The site is located in northwest of Xingtai and nestled in the Taihang Mountains. Agricultural crops surround the site, consisting heavily of winter wheat planted in

October and harvested in June (J. Liu & Si, 2011). Xingtai is a city with approximately 7 million people and is surrounded by industry including coal mining and coal-burning power plants, cement and steel industries, chemical processing, iron-smelting, and glass manufacturing.

2.2 Estimates of VOC Reactivity

Various reactivity scales have been used to assess the role of VOCs on O₃ formation, such as OH reactivity, the estimation of OFP and POCP, and observational and chemical transport models (Atkinson & Arey, 2003; Carter, 2010, 1994; Derwent et al., 1996; Finlayson-Pitts & Pitts, 1999).

2.2.1 OH Reactivity

Since the reaction with OH accounts for the majority of loss of VOCs, the rate constant for the reaction between OH and the hydrocarbon reflects the overall reactivity of that hydrocarbon (Finlayson-Pitts & Pitts, 1999). OH reactivity is defined by:

$$OHR(VOC_i) = k_{OH+VOC_i} * [VOC_i]$$

Reaction rate constants were obtained from the Master Chemical Mechanism version 3.3.1 (MCM3.3.1). If rate constants were not available, the National Institute of Standards and Technology (NIST) Chemical Kinetics database (www.kinetics.nist.gov/) was used. The faster hydrocarbons react with OH, the faster RO₂ and HO₂ are produced and the faster NO is oxidized to NO₂. However, the initial rate of OH attack does not reflect products and their production of further free radicals.

2.2.2 Ozone Formation Potential

MIR (unit: g O₃ formed/ g VOC) values have been calculated based on model simulations that were evaluated with smog chamber measurements (Carter, 1994). Observationally derived MIR values are difficult to obtain because fast response O₃ and VOC data are required (Stroud et al., 2008). OFP (ppbv O₃) is calculated by:

$$\boxed{OFP(VOC_i) = MIR_{VOC_i} * [VOC_i]}$$

MIR values from Carter (2010) are used in this analysis. This method is only valid when the VOC/NO_x ratio is low and gives an estimate of only the first 24 hours after initial release. The median VOC/NO_x ratio for all WAS was 6.03 ppbv/ppbv. Box modeling including oxygenated species indicates a large range of VOC/NO_x ratios ranging from 7 to 100 ppbv/ppbv. In comparison, the ratio of reactive organic gas to NO_x (ROG/NO_x) in Los Angeles is 7.6 ppbv/ppbv (Carter, 1994).

VOCs experience photochemical loss from emission sources near the surface to measured aloft concentrations. Estimation of OFP from aircraft observations throughout the PBL evaluates how O₃ formation is different from the surface. Thus, initial mixing ratios of VOCs must be considered if O₃ abatement measures are to be implemented (Xie et al., 2008).

2.2.3 Photochemical Ozone Creation Potential (POCP)

The POCP for a particular VOC species is determined by quantifying the effect of a small change in the VOC concentration on O₃ formation along a trajectory relative to an increase in the emission of the reference VOC over multiple days (Saunders et al., 2003). Ethylene, one of the most important O₃ precursors with medium reactivity with OH, is

chosen as a reference due to its well characterized chemical degradation products (Cheng et al., 2010). The POCP for a given VOC species can be calculated by:

$$POCP_i = \frac{\text{Ozone increment with } VOC_i}{\text{Ozone increment with ethylene}} \times 100$$

In this study, POCP values from Cheng et al. (2010) in the Pearl River Delta (PRD) were used. The POCP values for each VOC were calculated by separate model experiments with each having 6.8% of the total integrated VOC emission across the total model domain above the base case simulation (Cheng et al., 2010). The model was initialized with typical autumn conditions associated with photochemical pollution episodes in southeast China. Since previous studies have largely determined the PRD is sensitive to VOCs (Cheng et al., 2010; Shao et al., 2009), similar to the NCP, the usage of the derived values in the PRD should be appropriate for this study. Similar to previous studies, alkanes and oxygenated organic compounds have relatively low POCP values, while alkenes and aromatics have higher values (Cheng et al., 2010; Derwent et al., 1996; Saunders et al., 2003). A comparison MIR and POCP values used in this study shows that these two methods agree in general.

2.3 Identification of VOC Sources

Correlations between individual VOC species and with CO can be used to examine the major sources of ambient VOCs (Barletta et al., 2005; L. Li et al., 2015). In this study, we examined the correlations and ratios for certain VOC species and compared them to published emission ratios. Because there are 27 samples, we determined the degrees of freedom to be at least 18 by sample-to-sample autocorrelation analysis. Values are only shown when significant with 95% confidence (p-value < 0.05).

Several VOC indicator ratios, including benzene/toluene (B/T), m/p-xylene/o-xylene, and acetylene/ethane, were used in source identification (Barletta et al., 2005; Borbon et al., 2001; L. Li et al., 2015). Not all VOC species were used for source apportionment analysis due to large number of VOCs detected, some of which were sometimes below the detection limit.

2.4 Box Model Simulations

An observation-constrained box model called Framework in 0-Dimensional Atmospheric Modeling (F0AMv3.1) with the Carbon Bond Mechanism, version 6, revision 2 (CB6r2) was used in this study to evaluate oxidation processes during seven flights in the ARIAs campaign (Wolfe et al., 2016). The box model simulations covered the Y-12 flight tracks and the A²BC supersite in Xingtai (where the Y-12 conducted spirals) and constrained by observed NO₂, CO, and O₃. For each 1-minute flight data interval, the model was run with a 1-hour time step for 5 days in “solar cycle” mode to allow calculated reactive intermediates to achieve steady state. For every 5-minute ground data interval, the model was run with a 1-hour time step run with changing solar zenith angle calculated for the location of ground observations. A physical loss lifetime using dilution parametrization was set to 24 hours. Ground observations were only used for days that a flight occurred. Data was filled with the monthly average observations of NO₂ for May 15 and 17 and NO for June 11 due to missing surface measurements.

Periodic missing Y-12 NO₂ data due to internal auto-zeroing was linearly interpolated since gaps were short (~2 minutes). Due to the limited number of grab canisters per flight, VOCs were constrained based on determined boundary layer height for each flight. Boundary layer height was determined from potential temperature and

water vapor vertical profiles. Below the boundary layer, the samples from the research flights (RFs) were averaged and above the boundary layer (the free troposphere, FT) samples from all RFs were averaged. The average measured total VOC concentration in the PBL was ~20 ppbv and the average FT concentration was ~11 ppbv. The average concentration of the samples below 500 m was used as ground concentrations since A²BC did not measure VOCs at the surface. ARIAs also did not measure photolysis frequencies, so j-values were calculated as a function of solar zenith angle, altitude, O₃ column, and albedo using lookup tables calculated from the NCAR Tropospheric Ultraviolet and Visible (TUV) version 5.2 radiation model and cross sections and quantum yields documented in the literature (FOAM's "hybrid" method).

Unlike a 3-dimensional chemical transport model, the box model simulations do not include advection or emissions. These processes, while important, are not included in the box model since O₃ precursors were measured and used to constrain the model calculations. Box modeling is used to gain an understanding of O₃ production and its sensitivity to NO_x and VOCs using measured species and meteorological parameters in order to calculate O₃ production rates.

2.4.1 Ozone Production and Sensitivity Calculations

Ozone production during the daytime is determined by the production rate of NO₂ molecules from the HO₂+NO and RO₂+NO reactions subtracted from the loss mechanisms (Finlayson-Pitts & Pitts, 1999). Thus, the net O₃ production rate, net(PO₃) can be estimated as:

$$net(O_3) = k_{HO_2+NO}[HO_2][NO] + \sum_{i=1}^n k_{RO_{2i}+NO}[RO_{2i}][NO] - P(RONO_2)$$

$$-k_{OH+NO_2+M}[OH][NO_2][M] - k_{HO_2+O_3}[HO_2][O_3] - k_{OH+O_3}[OH][O_3] \\ -k_{O(^1D)+H_2O}[O(^1D)][H_2O] - L(O_3 + alkenes)$$

where k is the different reaction rate coefficients and RO_{2i} is the individual organic peroxy radicals. The terms subtracted from the production of O₃ are the loss mechanisms: the formation of nitrates, P(RONO₂), the reaction of OH and NO₂ to form nitric acid, the reaction of OH and HO₂ with O₃, the reaction of O(¹D) with H₂O, and the reactions of O₃ with alkenes. An additional term not included here is the rate of O₃ loss by dry deposition.

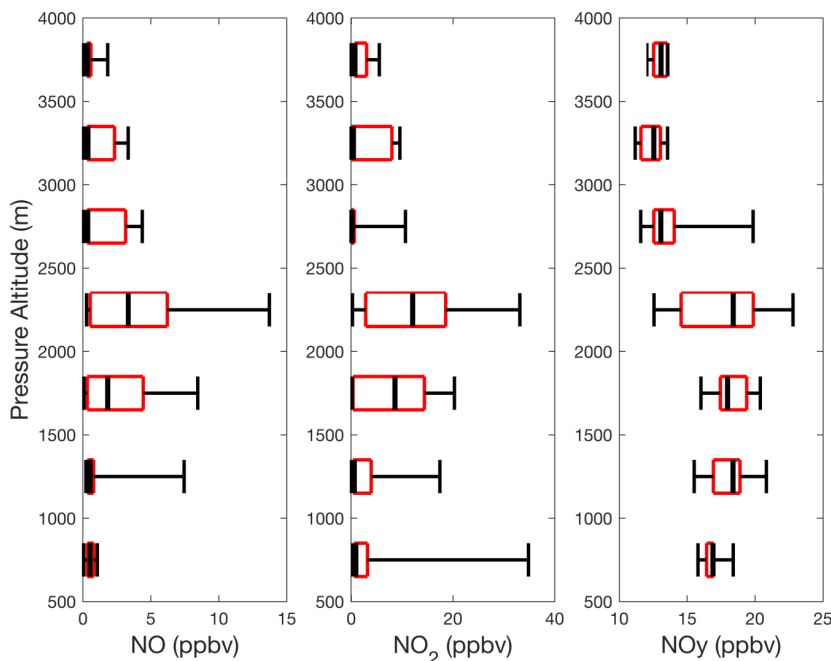
O₃ sensitivity was evaluated using the ratio of L_N/Q, where L_N is the radical loss through reactions with NO and Q is the primary radical production (Kleinman, 2005a). When L_N/Q is much less than 0.5, the O₃ production regime is NO_x-limited; when L_N/Q ratio is much higher than 0.5, the regime is VOC-limited. However, different environments have contrasting amount of organic nitrates which impacts the cutoff value, so this value could vary around 0.5 (Kleinman, 2005b).

Chapter 3. Results

3.1 Nitrogen Oxide Observations

We report average concentrations with \pm one standard deviation for NO_x observations. The average measured Y-12 NO concentration was 1.19 ± 2.01 ppbv, with a median of 0.57 ppbv. The median vertical profile of NO shows highest concentrations between 2000 and 2500 m of ~ 5 ppbv (Figure 3.1). We only report measured NO on half of the flights due to power constraints. Average NO_2 from the Y-12 at all altitudes during ARIAs was 3.00 ± 4.92 ppbv and median NO_2 was 1.28 ppbv. Similar to NO, the median NO_2 vertical profile peaked at ~ 10 ppbv between 2000 and 2500 m. The average NO_y concentration was 16.9 ± 2.94 ppbv, with a median of 17.4 ppbv. The altitude where NO_y peaked at ~ 17 ppbv was also between 2000 and 2500 m. The average lower free troposphere (>3000 m) NO_2 and NO concentrations measured during ARIAs was $0.13 \pm$

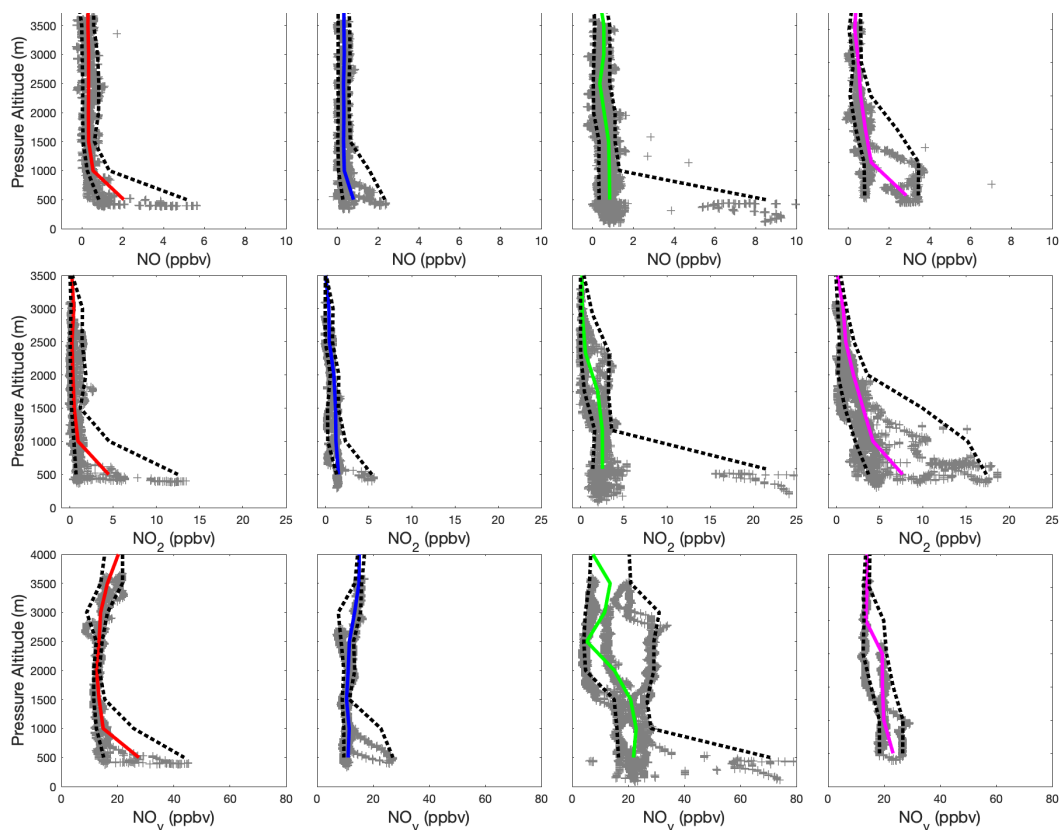
Figure 3.1: Altitude profiles of NO (left), NO_2 (middle), and NO_y (right) averaged every 500 m. The whiskers show the 5th and 95th percentiles; the red box edges show 25th and 75th percentiles and the central black line indicates the median.



Average O_3 at all altitudes from the Y-12 during ARIAs was 85.0 ± 15.6 ppbv and the median was 83.4 ppbv.

Observations above the Xingtai supersite measured the highest mean NO, NO_2 , and NO_y concentrations of 1.06 ppbv, 3.85 ppbv, and 18.5 ppbv, respectively, compared to the other spiral locations. Additionally, Xingtai observed the largest variation in near-surface CO concentrations. Quzhou observed the lowest concentrations of NO_2 , less than 1 ppbv. The vertical profiles of these species over the spiral locations (Figure 3.2), shows highest values observed closer to the surface (~ 500 m), particularly in the large urban

Figure 3.2: Median profiles of NO (top), NO_2 (middle) and NO_y (bottom) at four locations: Julu (red), Quzhou (blue), Shijiazhuang (green), and Xingtai (pink). Grey points are all data and the dashed black lines indicate the 5th and 95th percentiles. All units are ppbv.



center of Xingtai. The largest variability between 5th and 95th percentiles occurred primarily below 1000 m for all species.

3.2 Volatile Organic Compounds

3.2.1 Observations

The lowest sum of the volume mixing ratio of each VOC compound (total VOC mixing ratio) was 7.44 ppbv and the highest was 259.0 ppbv. The mean and median total VOC mixing ratio were 25.3 ppbv and 13.8 ppbv, respectively. The two lowest total VOC mixing ratios were collected at altitudes in the lower free troposphere (about 3500 m) on May 15 and June 2 about 14:00 local time. The largest total VOC mixing ratio was measured on May 21 in the early afternoon at a low altitude of approximately 400 m over Quzhou and will be referred to as the anomalous sample (Figure S4). This sample represents a parcel of heavily polluted air with little dilution due to the presence of chemical and agricultural production facilities. About 69% of the total VOC (180 ppbv) of the anomalous sample came from alkanes, with isopentane contributing for one-third of the total alkane mixing ratio (59.7 ppbv). Aromatics constituted 21% of the total mixing ratio of the anomalous sample (53.5 ppbv), with toluene accounting for 76% of the total aromatic mixing ratio (41.1 ppbv). Alkenes/alkynes and halocarbons accounted for 6% (16.5 ppbv) and 4% (9.68 ppbv) of the total VOC mixing ratio, respectively, of the anomalous sample, with vinyl chloride accounting for 35% of the total halocarbon mixing ratio (3.36 ppbv) and 1-butene accounting for 72% of the total alkene/alkyne mixing ratio (11.87 ppbv). This sample also documented high CFC-11, HCFC-22, CFC-114 above background concentrations (0.32 ppbv, 1.05 ppbv, and 0.55 ppbv, respectively). We included the anomalous sample and the samples collected in the lower

FT because the concentrations are representative of the region as a whole and percentile calculations are insensitive to removal of these outliers.

Investigation of the toxicity of VOCs reveals n-hexane, styrene, m/p/o-xylene, toluene, and benzene contribute ~20% (600 ppbC) of the total VOC mixing ratio, with over half of the mixing ratio due to the anomalous sample. This is suggestive of sampling chemical and agricultural production facilities from the anomalous sample, stressing the importance of quantifying hazardous VOCs.

3.2.2 Levels and speciation of VOCs

Table 3.1 summarizes the 15 most abundant NMHCs and HHs in terms of median volume mixing ratio, along with the percentage contribution to the sum of the volume mixing ratio of each VOC compound to the total (total VOC mixing ratio) and the percentage contribution to the sum of the volume mixing ratio of the VOC to the total of group (total speciated mixing ratio). Alkanes, alkenes/alkynes, aromatics, and halocarbons are responsible for 61%, 9%, 24%, and 6%, respectively, of the total ppbC mixing ratio. Alkanes made up 55% of the total VOC volume mixing ratio, with ethane, propane, isobutane, and isopentane making up ~70% of the total alkane volume mixing ratio. Halocarbons make a significant portion of the total VOC volume mixing ratio of approximately 18% of total. Vinyl chloride accounts for approximately 29% of the total halocarbon volume mixing ratio. Aromatics and alkenes/alkynes both made up ~13% of the total volume VOC mixing ratio. Toluene dominates the total aromatic volume mixing ratio by contributing approximately 60% to the total, while ethylene represents the largest alkene/alkyne volume mixing ratio of approximately 30%.

Table 3.1: Top 15 species ranked by median volume mixing ratio (Unit: ppbv) as well as mass concentration (Unit: $\mu\text{g}/\text{m}^3$) and percentage contribution to total VOC mixing ratio and speciated mixing ratio during ARLAs.

Ranking	Species	Median Volume Mixing Ratio	Median Concentration, $\mu\text{g}/\text{m}^3$	% Contribution to Total VOC Mixing Ratio	% Contribution to Total Speciated Volume Mixing Ratio
1	Ethane	2.55	3.43	10.7	19.4
2	Propane	1.38	2.72	5.74	44.6
3	Vinyl chloride	1.20	3.34	5.10	28.6
4	Chloromethane	1.03	2.32	4.27	23.9
5	Acetylene	0.67	0.77	3.90	30.3
6	CFC-12	0.56	3.04	2.32	13.0
7	Propylene	0.46	0.86	1.85	14.4
8	Ethylene	0.44	0.54	3.66	28.5
9	HCFC-22	0.37	1.42	1.67	9.37
10	Benzene	0.34	1.20	2.10	14.6
11	Toluene	0.30	1.24	8.95	62.4
12	CFC-11	0.28	1.74	1.47	8.27
13	Isobutane	0.26	0.68	6.44	11.7
14	1-Butene	0.26	0.65	3.11	24.2
15	Isopentane	0.19	0.61	11.5	20.9

3.2.3 OH Reactivity

The top 15 most influential NMHCs and HHs ranked by median OH reactivity along with the percent contribution to the sum of the OH reactivity of each VOC compound (total OH reactivity) and the percent contribution to the sum of the OH reactivity in the group (speciated OH reactivity) are shown in Table 3.2. While CO and CH₄ together contribute 33% to total OH reactivity, these species are removed from the analysis in order to focus on NMHC and HH reactivity.

Alkenes/alkynes account for 38% of the total OH reactivity, with 1-butene and propylene together accounting for 70% of the total alkene/alkyne OH reactivity. Alkanes and aromatics contribute 34% and 20% to total OH reactivity, respectively. While alkanes are generally the most abundant class of NMHCs, their relatively slow reaction rate with OH often makes their contribution to secondary pollutants less significant than the faster reacting unsaturated species. Halocarbons are the smallest contributors to total OH reactivity (8%), with vinyl chloride accounting for the majority of the halocarbon OH reactivity—over 96%.

Table 3.2: Top 15 species ranked by median OH reactivity (s^{-1}) and percentage contribution to total OH reactivity and speciated OH reactivity during ARIAs.

Ranking	Species	Median OH Reactivity, s^{-1}	% Contribution to Total OH reactivity	% Contribution to Speciated OH reactivity
1	Propylene	0.31	9.47	24.8
2	Vinyl chloride	0.22	7.57	96.3
3	1-Butene	0.19	18.3	47.9
4	Ethylene	0.09	5.75	15.1
5	Isoprene	0.05	2.61	6.84

6	Toluene	0.04	9.38	47.5
7	Propane	0.03	1.01	2.94
8	m/p-Xylene	0.03	4.29	21.7
9	1,2,4-Trimethylbenzene	0.02	0.71	3.59
10	Isopentane	0.02	7.79	22.8
11	2-Methylheptane	0.01	7.10	20.8
12	Ethane	0.01	0.41	1.19
13	Acetylene	0.01	0.52	1.37
14	Isobutane	0.01	2.50	7.31
15	Styrene	0.01	1.00	5.04

3.2.4 Ozone Formation Potential (OFP)

The top 15 most influential NMHCs and HHs ranked by median OFP along with the percent contribution to the sum of the OFP of each VOC compound (total OFP) and the percent contribution to the sum of the OFP in the group (speciated OFP) are shown in Table 3.3. Despite contributing large amounts to total mixing ratio and OH reactivity, CO and CH₄ contribute ~18% to total OFP due to low reactivities compared to other VOC species. If CO and CH₄ concentrations above background are considered, CH₄ has even less of an influence, only contributing ~3% to the total CH₄ OFP. CO contributes more, over 50% of the total CO OFP is due to concentrations above background.

The top 15 most influential NMHCs and HHs to OFP differ substantially from those representing emissions, explained by the differences in reactivity by MIR. Alkanes, alkenes/alkynes, aromatics, and halocarbons contribute 30%, 26%, 38%, and 7%, respectively, of total OFP. While aromatics contributed the most to OFP, the

corresponding volume-based contribution was only 14%. In contrast, alkanes contributed over 50% to total volume mixing ratio, but only comprise 30% of the total OFP. Toluene, 1-butene, and isopentane account for about 40% of the top 15 species to median OFP.

Table 3.3: Top 15 species ranked by median ozone formation potential (ppbv O₃) using maximum incremental reactivity (MIR) and percentage contribution to total OFP and speciated OFP during ARIAs.

Ranking	Species	Median Ozone Formation Potential, ppbv O ₃	% Contribution to Total OFP	% Contribution to Speciated OFP
1	Propylene	4.67	6.04	23.6
2	Vinyl chloride	4.41	6.00	89.7
3	1-Butene	2.95	11.3	44.3
4	Toluene	2.32	21.9	58.0
5	Ethylene	2.29	6.16	24.0
6	m/p-Xylene	1.10	6.93	18.3
7	Propane	0.62	0.83	2.76
8	1,2,4-Trimethylbenzene	0.51	0.88	2.32
9	o-Xylene	0.49	2.41	6.37
10	Ethane	0.45	0.60	2.00
11	Isopentane	0.41	8.02	26.8
12	Benzene	0.40	0.79	2.08
13	Isobutane	0.39	3.06	10.3
14	1,2,3-Trimethylbenzene	0.39	0.69	1.82

15	Acetylene	0.34	0.64	2.51
----	-----------	------	------	------

3.2.5 Photochemical Ozone Creation Potential

The top 15 most influential NMHCs and HHs ranked by median POCP along with the percent contribution to the sum of the POCP of each VOC compound (total POCP) and the percent contribution to the sum of the POCP in the group (speciated POCP) are shown in Table 3.4. POCP values for CO and CH₄ were not given in Cheng et al. (2010) and are excluded in the calculation.

Alkanes, alkenes/alkynes, aromatics, and halocarbons contribute 40%, 31%, 18% and 11% to total POCP, respectively. Vinyl chloride is responsible for over 90% of the total halocarbon POCP while ethylene and propylene are responsible for over half of the total alkene/alkyne POCP.

Table 3.4: Top 15 species ranked by median POCP-weighted mixing ratio (ppbv) and percentage contribution to total POCP and speciated POCP during ARIAs.

Ranking	Species	Median POCP-weighted Mixing Ratio, ppbv	% Contribution to Total POCP	% Contribution to Speciated POCP
1	Vinyl chloride	0.81	10.23	93.9
2	Propylene	0.73	8.72	28.1
3	Ethylene	0.44	10.8	34.8
4	1-Butene	0.26	9.37	30.2
5	Ethane	0.23	2.84	7.05
6	Propane	0.18	2.20	5.48
7	Toluene	0.11	9.50	53.1
8	Isobutane	0.07	5.32	13.2

9	Isopentane	0.07	11.9	29.5
10	m/p-Xylene	0.06	3.75	21.0
11	1,2,4-Trimethylbenzene	0.04	0.65	3.64
12	Acetylene	0.04	0.69	2.23
13	Isoprene	0.04	0.71	2.30
14	Cis-1,2-Dichloroethylene	0.03	0.41	3.78
15	2-Methylpentane	0.03	1.53	3.82

3.2.5.1 Comparison of OFP and POCP

The most reactive NMHCs and HHCs from OFP and POCP can be compared to assess differences in the scales. Aromatics contributed the most to OFP (38%), while POCP show alkanes (40%), closely followed by alkenes/alkynes (31%) to have the largest effect. The ranked species were very similar; small discrepancies lie with POCP values placing certain alkanes like propane above more reactive compounds in terms of MIR like o-xylene and ethylbenzene. This is likely due to the larger mean volume mixing ratio than a reflection of the reactivity itself.

The top 10 species ranked by MIR defined by Carter (2010), show these compounds contribute 33% to total OFP but only represent 10% of the total volume mixing ratio. Comparably the top 10 species ranked in terms of POCP defined by Cheng et al. (2010) shows these species contribute 21% to total POCP but represent 5% of the total volume mixing ratio. Previous studies in China found the top 15 OFP species (including m/p-xylene, toluene, propene, o-xylene, and ethylbenzene) contribute 69% of total OFP, but only account for 30% of the total emission (Liang et al., 2017). This suggests that species

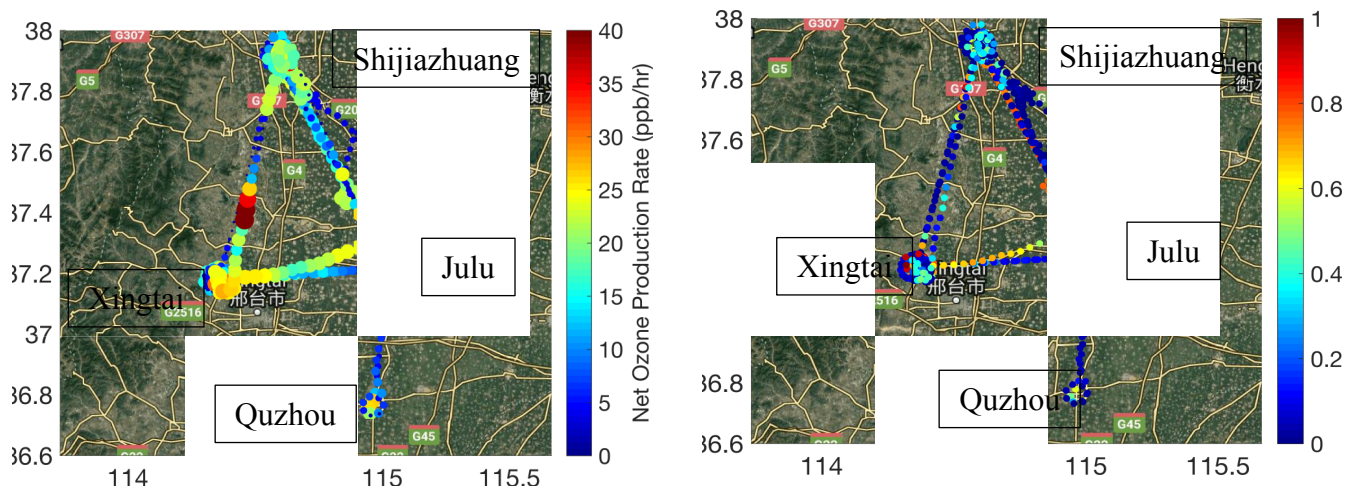
with either high reactivity or large emissions do not necessarily have high contributions to O₃ formation.

The most reactive individual species in terms of OFP and POCP was trans-2-butene (MIR=15.16, POCP=229), contributing 0.05 ppbv O₃ to OFP and 0.007 ppbv to POCP. Contrary to reactivity, propane accounted for a relatively high percentage of total mean mixing ratio by volume (5.74%) yet had negligible contribution toward OFP (0.83%) due to its low reactivity (MIR=0.49) and slightly higher contribution to POCP (2.20%). These results confirm that both reactivity scales and emissions rates must be considered together when formulating O₃ control strategies.

3.3 Photochemical Ozone Production Rate and Sensitivity

Ozone production rates calculated from the box model are high in major urban centers, particularly Shijiazhuang, Xingtai, and Julu, and Quzhou, but also between these cities (Figure 3.3). The largest net O₃ production rate over 40 ppbv/hour was located along the Taihang Mountains between Shijiazhuang and Xingtai. These large net

Figure 3.3: Left: Net O₃ production rate calculated using box model results along the Y-12 flight track during ARIAs. The size of the dots is proportional to the production rate of O₃. Right: O₃ production sensitivity indicator, L_N/Q , along the Y-12 flight track during ARIAs. Ozone production is VOC-sensitive when $L_N/Q > 0.5$ and NO_x-sensitive when $L_N/Q < 0.5$.

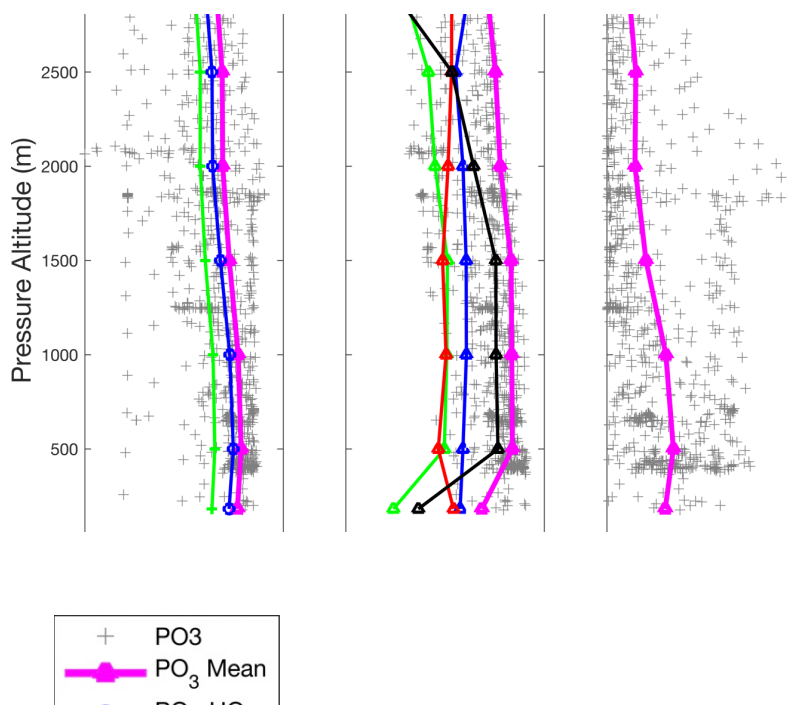


production rates occurred ~2000 m on June 11 when NO, NO_y, NO₂, and O₃ were 0.51 ppbv, 16.29 ppbv, 2.14 ppbv, and 83.64 ppbv, respectively. Total VOC mixing ratios of the WAS closest in time and altitude near this peak of net O₃ production rates was ~30 ppbC.

L_N/Q values indicate O₃ production rates were mostly NO_x-sensitive at high altitudes over the NCP and more VOC-sensitive at lower altitudes near urban centers (Figure 9). Vertical profiles of O₃ production, loss, and net rates using the box model results (Figure 3.4) show that HO₂+NO makes more O₃ than RO₂+NO during the campaign, the major loss of O₃ is due to the termination of NO₂ through its reaction with OH below 2500 m, and a maximum of net O₃ production was observed in the lowest 500 m of ~13 ppbv/hour. In the PBL, mean net O₃ production rates reached ~5 ppbv/hour and in the lower free troposphere, mean net O₃ production rates were still ~2 ppbv/hour and conducive to long-range transport. A follow-up paper will investigate export to Korea where the KORUS-AQ experiment was underway (e.g. Huang et al., 2018).

Figure 3.4: Vertical profiles of the O₃ production rate (left), O₃ loss rate (middle), and net O₃ production rate (right) during ARIAs.

3.4 Comparison to Colorado Front Range experiment: FRAPPÉ



The Colorado Front Range experiment, FRAPPÉ, consisted of a series of coordinated research flights and ground-based measurements. We filter data for 8-16 LT and below 4 km to better compare with ARIAs observations. FRAPPÉ VOC measurements on board the C-130 are collected by WAS flasks, the trace organic gas analyzer (TOGA), and proton transfer reaction-mass spectroscopy (PTR-MS). In this study, we characterize alkanes, alkenes, alkynes, and halocarbons collected from WAS analyzed using an Advanced Whole Air Sampler (AWAS) and oxygenated organics using TOGA. The WAS are sent for analysis by gas chromatography (GC) with flame ionization detection (FID), electron capture detection (ECD) and mass spectrometric detection (MSD) at the University of California-Irvine and identified and quantified for

more than 70 trace gases. Experimental procedures have been well documented based on numerous prior field missions including in China (Barletta et al., 2009; Blake et al., 1999, 2001, 2003, 2004, 2008, Simpson et al., 2001, 2003, 2010, 2011). Details on TOGA are summarized elsewhere (Apel et al., 2003)

FRAPPÉ completed flights in two regions of the Front Range: Weld County located northeast of Denver, an area of oil and natural gas operations, and the larger Denver metropolitan area with urban emissions (Pfister et al., 2017). Since flight coverage was not equal, we divide the Front Range into these two regions.

3.4.1 Nitrogen Oxide Observations

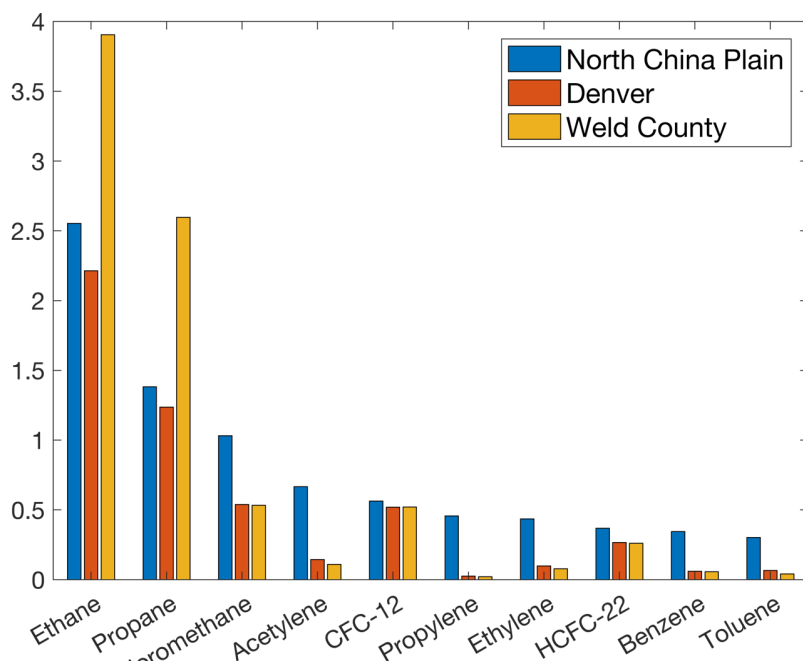
Average and median volume mixing ratios of NO and NO₂ are larger in Denver than Weld County. The average measured C-130 NO and NO₂ mixing ratios are 0.72 ± 2.20 ppbv and 2.03 ± 4.60 ppbv in Denver and 0.21 ± 0.29 ppbv and 0.77 ± 1.07 ppbv in Weld County. This is about 0.5-1.0 ppbv of NO and ~1 ppbv NO₂ smaller than in the NCP. Above 3000 m, average NO and NO₂ is 0.44 ± 0.73 ppbv and 1.42 ± 2.04 ppbv in Weld County and 0.15 ± 0.21 and 0.59 ± 0.64 ppbv in Denver. In the average lower free troposphere, NO in Weld County is comparable to the NCP, while about 0.25 ppbv lower in Denver. Lower FT NO₂ is higher in both locations in the FR compared to the NCP.

3.4.2 Volatile Organic Compounds

The range of species measured during FRAPPÉ were comparable to ARIAs but included oxygenated organics (OOs). The most important source of OOs in the atmosphere is oxidation of hydrocarbons (Mellouki et al., 2015). Oxygenated species are included here to evaluate their impact on O₃ production, while such data were not available during ARIAs. However, F0AM estimates a 20% contribution due to OOs to

Figure 3.5: Median mixing ratios (ppbv) of the top 10 species contributing to total VOC mixing ratio in China (blue). Median values measured during FRAPPÉ in Denver and Weld County are shown in red and yellow.

A comparison of the top 10 species by median volume mixing ratio in the NCP to



median values in Denver and Weld County (Figure 3.5) shows light alkanes, like ethane and propane, are enriched in Weld County compared to the NCP. Vinyl chloride was not measured in FRAPPÉ. Alkenes, such as propylene and ethylene, and aromatics, like benzene and toluene, are greater in median volume mixing ratio in the NCP compared to the Front Range. Chloromethane is a factor of 2 higher in ARIAs compared to FRAPPÉ,

while median CFC-12 and HCFC-22 is slightly elevated by ~40 pptv and 100 pptv, respectively, in the NCP compared to the FR.

Table 3.5 and Table 3.6 summarize the top 5 NMHCs by mean volume mixing ratio, OH reactivity, OFP, and POCP in Denver and Weld County. Notably, measured oxygenated compounds make up large contributions to total volume mixing ratio, total OH reactivity, total OFP, and total POCP, suggesting that OOs might also be important in China.

OOs constitute the majority of total volume mixing ratio in both Denver (85%) and Weld County (73%), with methanol contributing ~30% to the total volume mixing ratio of VOCs in both locations. A larger contribution due to ethane is observed in Weld County (8.99% of the total compared to 4.63% of the total in Denver) due to the prevalence of oil and natural gas operations. Excluding OOs, alkanes, alkenes/alkynes, aromatics, and halocarbons contribute 88%, 2%, 2%, and 8% in Weld County and 81%, 5%, 2%, and 12% in Denver.

OOs also have a large influence on OH reactivity in Denver and Weld County (87% and 79%, respectively, of the total OH reactivity), with formaldehyde and acetaldehyde accounting for ~50% of the total OH reactivity for both locations. Isoprene in the Front Range is within the top 10 species contributing to OH reactivity, but its relative contribution to OH reactivity is smaller compared to the NCP (1.8% in Denver, 1.3% in Weld County, and 2.6% in the NCP). When the OOs are removed, alkanes, alkenes/alkynes, and aromatics contribute 72%, 25%, and 3% in Weld County and 53%, 38%, and 8% in Denver. Halocarbons contributed very small amounts to OH reactivity during the FR campaign.

OOs also constitutes 80-90% of the OFP and POCP in Denver and Weld County, with formaldehyde and acetaldehyde often in the top 2 for both scales in both locations. Methanol, produced by oil and natural gas operations, is also influential in O₃ production. However, Weld County shows a higher influence of alkanes on OFP (13% vs. 6%) and POCP (17% vs. 8%). Ethane, propane, and n-butane are responsible for much of this discrepancy due to oil and natural gas operations present in Weld County. OFP and POCP values for ethane and propane are a factor of 2 higher in Weld County than in Denver, suggestive of the large influence oil and natural gas operations has on O₃ production in this region. When OOs are excluded, alkanes and alkenes/alkynes are the dominant contributors to OFP and POCP. However, the contribution to OFP due to aromatics is larger in Denver than Weld County (17% vs. 7%).

Interestingly, halocarbons in FRAPPÉ are of little importance concerning OH reactivity, OFP, and POCP (< 1% for both locations), which was not the case during ARIAs. However, different halocarbons with varying reactivities were measured in these campaigns, not allowing for a direct comparison.

Table 3.5: The top 5 NMHCs measured during FRAPPÉ in Denver ranked by median volume mixing ratio, OH reactivity, OFP, and POCP. The percentage contribution to total and speciated volume mixing ratio, OH reactivity, OFP, and POCP are given in %.

Denver	Species	Median	% Contribution to Total	% Contribution to Speciated
Mixing Ratio (ppbv)	Methanol	5.00	33.3	39.0
	Acetic Acid	3.43	10.1	11.8
	Acetone	2.26	13.6	15.9

	Ethane	2.21	4.63	39.4
	Formaldehyde	1.79	11.4	13.3
OH reactivity (s⁻¹)	Formaldehyde	0.30	38.6	44.6
	Acetaldehyde	0.18	25.0	28.8
	Methanol	0.08	11.6	13.4
	Isoprene	0.06	1.78	34.3
	Acetic Acid	0.05	3.15	3.64
OFP (ppbv O₃)	Formaldehyde	10.6	44.7	50.2
	Acetaldehyde	3.73	16.4	18.5
	Acetic Acid	2.92	5.69	6.39
	Methanol	2.23	9.88	11.1
	Acetone	0.99	3.93	4.42
POCP (ppbv)	Formaldehyde	1.20	28.9	32.3
	Acetone	0.80	18.2	20.4
	Acetaldehyde	0.72	18.1	20.3
	Methanol	0.55	13.9	15.5
	Acetic Acid	0.21	2.29	2.56

Table 3.6: The top 5 NMHCs measured during FRAPPÉ in Weld County ranked by median volume mixing ratio, OH reactivity, OFP, and POCP. The percentage contribution to total and speciated volume mixing ratio, OH reactivity, OFP, and POCP are given in %.

Weld County	Species	Median	% Contribution to Total	% Contribution to Speciated
Mixing Ratio (ppbv)	Methanol	5.41	29.9	40.7
	Ethane	3.91	8.99	38.1

	Acetic Acid	2.82	8.58	11.7
	Propane	2.60	6.79	28.8
	Acetone	2.20	12.2	16.7
OH reactivity (s⁻¹)	Formaldehyde	0.28	34.6	44.0
	Acetaldehyde	0.21	23.2	29.5
	Methanol	0.10	11.2	14.2
	Propane	0.06	3.07	20.0
	n-Butane	0.05	3.17	20.6
OFP (ppbv O₃)	Formaldehyde	9.65	40.7	49.5
	Acetaldehyde	4.22	15.6	18.9
	Methanol	2.42	9.62	11.7
	Acetic Acid	2.40	5.26	6.40
	n-Butane	1.35	3.16	23.2
POCP (ppbv)	Formaldehyde	1.09	25.6	31.8
	Acetaldehyde	0.82	16.7	20.8
	Acetone	0.78	17.3	21.5
	Methanol	0.59	13.2	16.3
	Ethane	0.35	3.24	19.1

3.5 Major Sources of VOCs

During the ARIAs observation period, short-length alkanes (C₂/C₃) correlated well ethylene and benzene ($r > 0.80$, $p < 0.05$) A strong correlation between propane and propylene ($r=0.82$, $p < 0.05$) and the fact that propylene closely traces liquefied petroleum gas (LPG) alkanes, suggests propylene is linked to LPG car exhaust due to incomplete combustion leakage. However, strong correlations between ethylene,

propylene, 1-butene, tetrachloroethylene, and trichloroethylene, also exist, indicating production of synthetic rubber in the petrochemical industry.

The ratio of acetylene to ethane during ARIAs was 0.45 (Figure 3.6a) within the range of biomass burning of crop residue found from other studies in China (J. Chen et al., 2017). While wildfire events occurred during FRAPPÉ (Lindaas et al., 2017), low ratios in both regions in the Front Range suggest alternative sources of ethane and acetylene. Strong correlations of ethane and methane in Weld County ($r=0.87$, $p < 0.05$) and Denver ($r=0.89$, $p < 0.05$) is suggestive of oil and natural gas operations contributing to ethane sources in the FR, while strong correlations of acetylene with CO in both Denver ($r=0.95$, $p < 0.05$) and Weld County ($r=0.83$, $p < 0.05$) points to vehicular sources.

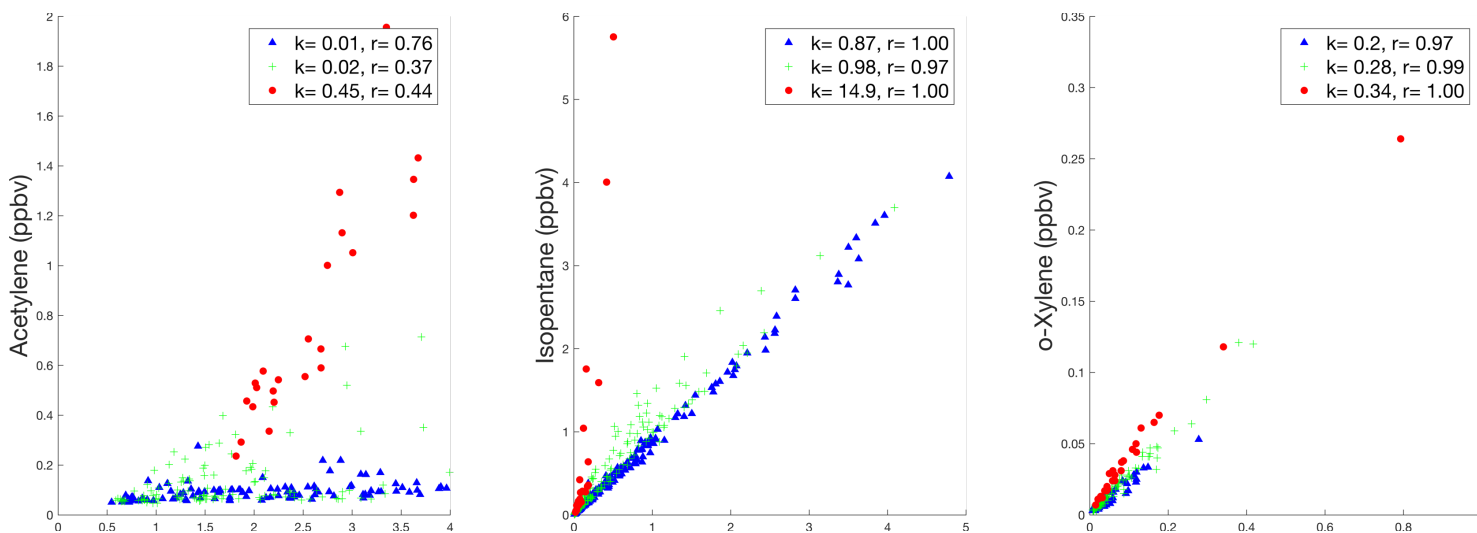
Isopentane correlates with a variety of alkane and aromatic species, indicative of gasoline evaporation in both the NCP and FR. The isopentane to n-pentane ratio in Weld County was less than 1, indicative of oil and natural gas operations (Figure 3.6b). The ratio in Denver was ~ 1 , suggestive of mixing processes throughout the Front Range. The large isopentane to n-pentane ratio during ARIAs persists with and without the anomalous sample and likely indicative of multiple isopentane sources including vehicular emission, gasoline evaporation and solvent evaporation.

Aromatic species such as m/p-xylene and o-xylene have been associated with vehicular emissions and solvents (H. Wang et al., 2014). During ARIAs, m/p-xylene and o-xylene correlated well ($r > 0.99$ with and without the anomalous sample) with a slope of 0.34 (Figure 3.6c). In a tunnel study in the Pearl River, the ratio of these aromatics was 0.35 (Y. Liu et al., 2008), consistent with our measurements. In comparison, in FRAPPÉ

the slope between o-xylene and m/p-xylene was between 0.2 and 0.28 ($r > 0.98$). These values are lower than observations in the Beijing-Tianjin-Hebei region (L. Li et al., 2015) with values between 0.32-0.48.

Small amounts of isoprene were observed in ARIAs (0.04 ± 0.04 ppbv) and FRAPPÉ (0.05 ± 0.07 ppbv) due to the low prevalence of broad-leaf trees in the regions where these campaigns were conducted and time of year (Guenther et al., 1993). Isoprene sources are mostly biogenic in the NCP and FR, but correlation with isopentane during ARIAs suggests a small anthropogenic contribution when the anomalous sample is excluded ($r = 0.42$, $p < 0.05$). A small correlation is observed in Denver and a slightly larger correlation is obtained in Weld County ($r = 0.42$, $p < 0.05$), suggestive of a minor anthropogenic component to isoprene sources in a major urban center.

Figure 3.6: Slope (k) and correlations (r) of (a) acetylene with ethane, (b) isopentane with n-pentane, and (c) o-xylene with m/p-xylene for ARIAs in China (all samples, red circles) and Weld County (blue triangles), and Denver (green crosses).



To distinguish between vehicular emission and other combustion sources throughout the different regions, the B/T ratio was used. Benzene was observed at high mean

concentrations over Hebei (0.53 ppbv vs. 0.08 ppbv in the FR). The average B/T ratio is 1.76 ± 1.60 ppbv/ppbv in the North China Plain, 1.60 ± 1.57 ppbv/ppbv in Denver, and 2.01 ± 1.35 ppbv/ppbv in Weld County. Table 9 summarizes the CH₄ enhancement for ARIAs and FRAPPÉ with varying B/T ratios using global mean CH₄ obtained from the Earth System Research Laboratory (ESRL) of NOAA for the months of ARIAs and FRAPPÉ. When the B/T ratio is less than 1, indicative of vehicular emissions, average CH₄ enhancements compared to the global mean is relatively small—103.6 ppbv for ARIAs and between 30-50 ppbv for FRAPPÉ. When B/T is greater than 1, the enhancement of CH₄ from ARIAs was about five times that of FRAPPÉ and the mean ethane volume mixing ratio is 2.78. This suggests influence of leakage from oil and natural gas operations, coal combustion, or biomass burning in Hebei Province. Contrary to ARIAs, the enhancement in CH₄ during FRAPPÉ is negligible. Benzene correlates with SO₂ ($r = 0.70$), CO ($r = 0.67$), and ethane ($r = 0.84$), all tracers from incomplete fossil fuel combustion. During FRAPPÉ, biomass burning and oil and natural gas operations are the main contributor to the high B/T ratio (Andreae & Merlet, 2001; Halliday et al., 2016; Moreira Dos Santos et al., 2004).

The lack of correlation of CO with various hydrocarbons in ARIAs suggests these compounds may have additional sources beyond evaporative and tailpipe emissions or that CO has an additional source. Ethane, benzene, and the substituted benzenes are the only species that correlate well and significantly with CO, all of which components of gasoline, coking, or tracers of incomplete combustion, like low technology coal combustion and biomass burning. Correlations with a variety of halocarbons with these tracers of incomplete combustion during ARIAs suggest collocation of VOC sources with

petrochemical and chemical facilities (Ryerson et al., 2003). Certain hydrocarbons like m/p-xylene, ethylene, 2-methylpentane, and isopentane during FRAPPÉ correlate better with CO, suggesting vehicular sources are largely responsible for emissions. Previous research has indicated industrial VOC emissions appear to be less important compared to mobile and oil and natural gas in the Front Range, but can have some significant impacts on the local scale (Pfister et al., 2017).

Table 3.7: Average CH₄ and enhancement compared to global monthly average for all data, data when benzene/toluene (B/T) > 1, and when benzene/toluene < 1 for ARIAs and FRAPPÉ.

	North China Plain, ppbv	Front Range, ppbv	Weld County, ppbv
Average Seasonal CH ₄	1969.1	1837.7	1853.4
Average CH ₄ B/T > 1	1985.9	1843.0	1846.0
Average CH ₄ B/T < 1	1945.7	1867.4	1847.9
Global Average CH ₄	1842.1	1815.4	1815.4
Enhancement All	127.0	22.3	38.0
Enhancement B/T > 1	143.8	27.6	30.6
Enhancement B/T < 1	103.6	52.0	32.5

Chapter 4. Discussion

Excluding HHs, we observed alkane (67%), alkene/alkyne (11%), and aromatic (17%) contributions to total volume mixing ratios similar to L. Li *et al.* (2015) surface observations in June and July 2014 in Quzhou (56.81%, 19.23%, and 11.41%, respectively). When halocarbons are included, alkenes and aromatics both contribute relatively low amounts to total mixing ratio, approximately 13%, while halocarbons supply 18% to the total VOC mixing ratio. Vinyl chloride, used in the production of the polymer polyvinyl chloride, is the most abundant halocarbon with an average volume mixing ratio of 1.28 ppbv and a standard deviation of 0.51 ppbv in the NCP. Previous studies in China have observed small mixing ratios of vinyl chloride (10-100 pptv) (Gu *et al.*, 2019; Ran *et al.*, 2011), while surface measurements at an industrial/petrochemical site in Korea observed much higher concentrations of 4.0 ± 1.8 ppbv (Na *et al.*, 2001). Prior studies have shown elevated vinyl chloride levels near landfills as high as 100 ppbv (Seiber, 1996), on subway stations in Shanghai as large as 788 pptv (Y. Zhang *et al.*, 2012), and in PVC plastic waste recycling plants in amounts as high as 35 ppbv (Tsai *et al.*, 2009). Vinyl chloride is not a major O₃ precursor in areas of traditional photochemical smog studies such as LA, the eastern US (Halliday *et al.*, 2015), or Japan (Okada & Nakagoshi, 2012) and this paper points to the role it has in the NCP.

When ranked by OH reactivity excluding HHs, our results were again similar to Li *et al.* (2015) with alkanes, alkenes/alkynes, and aromatics contributing 37%, 41%, and 21%, respectively to total OH reactivity. This study in the Beijing-Tianjin-Hebei region estimated alkene OH reactivity accounted for 35.7-40.7% of the total (L. Li *et al.*, 2015). 1-Butene was the largest contributors to total OH reactivity in the NCP, contributing ~18% of the total. Isopentane was the largest contributor of the alkanes to OH reactivity

during ARIAs, representing ~23% of the total alkane OH reactivity, closely followed by 2-methylheptane (20.8% of alkane OH reactivity). Unlike previous studies, isoprene was not among the top contributors to OH reactivity during ARIAs, instead contributing 2.56% of the total OH reactivity and 6.64% to total alkene OH reactivity.

Aromatics were the largest contributor to OFP, closely followed by alkanes and alkenes/alkynes. Excluding halocarbons, alkanes, alkenes/alkynes, and aromatics contributed 31%, 27%, and 41% to the total OFP, again comparable to values found by Li et al. (2015). Alkanes had the largest influence on POCP as a group, but specific species like propylene, vinyl chloride, and 1-butene were largely responsible for OFP and POCP. Propylene, a typical incomplete combustion species, is linked to propane likely from LPG car exhaust and also correlates with 1-butene, tetrachloroethylene, and trichloroethylene to produce synthetic rubber in the petrochemical industry (Lau et al., 2010). Vinyl chloride is also from petrochemical processes producing plastics. These results confirm that both reactivity scales and emissions rates must be considered together when formulating O₃ control strategies. After the control of NO_x, controlling aromatics, such as toluene and m/p-xylene, alkenes, like 1-butene, and certain halocarbons, particularly vinyl chloride, would have the greatest positive impact on O₃ abatement.

Alternatively, OOs likely from secondary sources compromised most of the mixing ratio, OH reactivity, and OFP and POCP during the FRAPPÉ campaign in both Denver and Weld County. While OOs are shown to play a major role in O₃ production in the Front Range, we have no evidence of a strong contribution in the NCP. Box model estimates suggest oxygenates contribute ~20% to the total VOC volume mixing ratio in the NCP, but were not measured during ARIAs. A prior study in Beijing in August 2005

found that about half of the C1-C3 aldehydes were attributed to secondary sources (Y. Liu et al., 2009). The largest species contributing to volume mixing ratio in the FR are methanol and ethane, whereas formaldehyde and acetaldehyde constitute the most towards OH reactivity and OFP. Isoprene contributes ~1.5% to the total OH reactivity in Denver and Weld County. Since the majority of OOs are produced, rather than emitted, the control of OO precursors is necessary for O₃ control.

Most of the light alkanes are greater by volume mixing ratio over the FR relative to the NCP but alkenes and aromatics are more enriched over China. Ethane, benzene, acetylene, and substituted benzenes have strong correlations with CO in both locations, which showcases the influence of transportation related emissions, biomass burning, and in China, low technology coal combustion. Ratios of vehicular tracers, such as o-xylene and m/p-xylene, show emissions ratios comparable to values from the literature of vehicular sources in China (Y. Liu et al., 2008). For ARIAs, control of vehicle exhaust emissions might facilitate control of ambient VOCs due to high correlation of the substituted xylenes. The alkane composition and correlation of VOCs with isopentane in the NCP and FR were comparable, suggesting vehicular emissions from tailpipe and gasoline evaporation were sources of selected VOCs. The correlation of incomplete combustion species with halocarbons in the NCP indicates collocation with petrochemical sources. Reduction of halocarbon emissions from plastic manufacturing or other sources releasing vinyl chloride in Hebei might also help control O₃. Noticeable CH₄ enhancement was detected during ARIAs, suggesting natural gas leakage, but not during FRAPPÉ. Despite similar ecological environments, location in the midlatitudes, and position near the mountains, ARIAs and FRAPPÉ have commonalities in VOC

emissions; however, a “one-solution” approach to VOC reduction will not effectively reduce O₃ production in both places.

Chapter 5. Conclusions

High concentrations of O₃ were observed over the NCP and in this study we investigate the origin of these smog events. Measurements of trace gases including O₃, NO_x, VOCs, CFCs, and aerosols were taken in May and June 2016. Twenty-seven samples analyzed for 74 VOCs and HHs were taken aboard a Y-12 research aircraft in the PBL. Major conclusions include:

1. Over Hebei concentrations of VOCs were high, with larger median mixing ratios of alkenes, like propylene and ethylene, and aromatics, such as benzene and toluene, than the FR. The Colorado FR, particularly Weld County, was richer in light alkanes such as ethane and propane than the NCP. Average levels of NO_x were larger in the NCP than the FR, but several ppbv of NO₂ above 3000 m in Denver is suggestive of the large variability of NO₂ above the PBL.
2. Concentrations of NO_x and VOCs throughout the PBL over nonurban parts of Hebei Province were high enough to generate O₃ at a peak rate of ~13 ppbv/hour below 500 m (PBL mean 5 ppbv/hour). The lower free troposphere up to ~3000 m was frequently polluted with CO and NO₂ averaging ~200 ppbv and ~100 pptv with peak O₃ production rates ~ 5 ppbv/hour (mean 2 ppbv/hour conducive to long-range transport).
3. Unlike the NCP, where aromatics, alkenes, and alkanes contribute the most to O₃ formation, oxygenated organics were a major player in the FR, with alkenes and

aromatics playing small roles. Halocarbons, particularly vinyl chloride, also contribute to O₃ production in the NCP, but not in the FR.

4. Ratios of various NMHCs such as acetylene to ethane, isopentane to n-pentane, and o-xylene to m/p-xylene indicate the presence of extensive biomass burning and vehicular emissions during ARIAs, while oil and natural gas operations are dominant during FRAPPÉ. The correlation of incomplete fossil fuel combustion tracers with halocarbons in the NCP may indicate collocation with petrochemical sources.

This paper shows in order to improve aloft O₃ concentrations in the NCP, NO_x and VOCs from petrochemical processes, vehicular emissions, and biomass burning sources and NO_x should be targeted. The control of aromatics, such as toluene and m/p-xylene, alkenes, like 1-butene, and certain halocarbons, such as vinyl chloride, would have the greatest positive impact on O₃ abatement. However, in the Front Range, oil and natural gas operations and vehicular emissions contribute to produce oxygenates like formaldehyde and acetaldehyde important in O₃ production. While similarities in sources between the NCP and FR are evident, it is apparent the same approach will not yield similar results when trying to control O₃. Future work will investigate greenhouse gases, ozone destroying halocarbons, the production potential of SOAs, and export of pollutants.

References

- Abeleira, A., Pollack, I. B., Sive, B., Zhou, Y., Fischer, E. V., & Farmer, D. K. (2017). Source characterization of volatile organic compounds in the Colorado Northern Front Range Metropolitan Area during spring and summer 2015. *Journal of Geophysical Research*, *122*(6), 3595–3613. <https://doi.org/10.1002/2016JD026227>
- Andreae, M. O., & Merlet, P. (2001). Emission of trace gases and aerosols from biomass burning. *Global Biogeochemical Cycles*, *15*(4), 955–966. <https://doi.org/10.1029/2000GB001382>
- Apel, E. C., Hills, A. J., Lueb, R., Zindel, S., & Eisele, S. (2003). A fast-GC / MS system to measure C 2 to C 4 carbonyls and methanol aboard aircraft, *108*. <https://doi.org/10.1029/2002JD003199>
- Atkinson, R., & Arey, J. (2003). Atmospheric Degradation of Volatile Organic Compounds. *Chemical Reviews*, *103*(3), 4605–4638. <https://doi.org/10.1021/cr0206420>
- Barletta, B., Meinardi, S., Rowland, F. S., Chan, C. Y., Wang, X., Zou, S., et al. (2005). Volatile organic compounds in 43 Chinese cities. *Atmospheric Environment*, *39*(32), 5979–5990. <https://doi.org/10.1016/j.atmosenv.2005.06.029>
- Barletta, B., Meinardi, S., Simpson, I. J., Atlas, E. L., Beyersdorf, A. J., Baker, A. K., et al. (2009). Characterization of volatile organic compounds (VOCs) in Asian and north American pollution plumes during INTEX-B : identification of specific Chinese air mass tracers. *Atmos. Chem. Phys*, (2), 5371–5388.
- Blake, N. J., Blake, D., Wingenter, O., Sive, B., Kang, C. H., Thornton, D. C., et al. (1999). Aircraft measurements of the latitudinal , vertical , and seasonal variations of NMHCs , methyl nitrate , methyl halides , and DMS during the First Aerosol Characterization Experiment (ACE 1) Nicola at Laboratory at Department of Chemistry , National of. *Journal of Geophysical Research*, *104*.
- Blake, N. J., Blake, D., Simpson, I., Lopez, J., Johnston, N., Swanson, A., et al. (2001). Large-scale latitudinal and vertical distributions of NMHCs and selected halocarbons in the troposphere over the Pacific Ocean during the March-April 1999 Pacific Exploratory. *Journal of Geophysical Research*, *106*.
- Blake, N. J., Blake, D. R., Swanson, A. L., Atlas, E., Flocke, F., & Rowland, F. S. (2003). Latitudinal, vertical, and seasonal variations of C1C4 alkyl nitrates in the troposphere over the Pacific Ocean during PEM-Tropics A and B: Oceanic and continental sources. *Journal of Geophysical Research*, *108*, 1–13. <https://doi.org/10.1029/2001JD001444>
- Blake, N. J., Streets, D. G., Woo, J., Simpson, I. J., Green, J., Meinardi, S., et al. (2004). Carbonyl sulfide and carbon disulfide : Large-scale distributions over the western Pacific and emissions from Asia during TRACE-P. *Journal of Geophysical Research*, *109*, 1–15. <https://doi.org/10.1029/2003JD004259>
- Blake, N. J., Campbell, J. E., Vay, S. A., Fuelberg, H. E., Huey, L. G., Sachse, G., et al.

- (2008). Carbonyl sulfide (OCS): Large-scale distributions over North America during INTEX-NA and relationship to CO 2. *Journal of Geophysical Research*, 113. <https://doi.org/10.1029/2007JD009163>
- Bo, Y., Cai, H., & Xie, S. D. (2008). Spatial and temporal variation of historical anthropogenic NMVOCs emission inventories in China. *Atmospheric Chemistry and Physics*, 8(23), 7297–7316. <https://doi.org/10.5194/acp-8-7297-2008>
- Borbon, A., Fontaine, H., Veillerot, M., Locoge, N., Galloo, J. C., & Guillermo, R. (2001). An investigation into the traffic-related fraction of isoprene at an urban location. *Atmospheric Environment*, 35(22), 3749–3760. [https://doi.org/10.1016/S1352-2310\(01\)00170-4](https://doi.org/10.1016/S1352-2310(01)00170-4)
- Brocco, D., Fratarcangeli, R., Lepore, L., Petricca, M., & Ventrone, I. (1997). Determination of aromatic hydrocarbons in urban air of Rome. *Atmospheric Environment*, 31(4), 557–566. [https://doi.org/10.1016/S1352-2310\(96\)00226-9](https://doi.org/10.1016/S1352-2310(96)00226-9)
- Cai, C. J., Geng, F. H., Tie, X. X., Yu, Q., Peng, L., & Zhou, G. Q. (2010). Characteristics of ambient volatile organic compounds (VOCs) measured in Shanghai, China. *Sensors*, 10(8), 7843–7862. <https://doi.org/10.3390/s100807843>
- Carter, W. P. . (2010). *Updated Maximum Incremental Reactivity Scale and Hydrocarbon Bin Reactivities for Regulatory Applications*.
- Carter, W. P. L. (1994). Development of Ozone Reactivity Scales for Volatile Organic Compounds. *Air & Waste*, 44(7), 881–899. <https://doi.org/10.1080/1073161X.1994.10467290>
- Chen, J., Li, C., Ristovski, Z., Milic, A., Gu, Y., Islam, M. S., et al. (2017). A review of biomass burning: Emissions and impacts on air quality, health and climate in China. *Science of the Total Environment*, 579(November 2016), 1000–1034. <https://doi.org/10.1016/j.scitotenv.2016.11.025>
- Chen, P., Quan, J., Zhang, Q., Tie, X., Gao, Y., Li, X., & Huang, M. (2013). Measurements of vertical and horizontal distributions of ozone over Beijing from 2007 to 2010. *Atmospheric Environment*, 74(August), 37–44. <https://doi.org/10.1016/j.atmosenv.2013.03.026>
- Cheng, H. R., Guo, H., Saunders, S. M., Lam, S. H. M., Jiang, F., Wang, X. M., et al. (2010). Assessing photochemical ozone formation in the Pearl River Delta with a photochemical trajectory model. *Atmospheric Environment*, 44(34), 4199–4208. <https://doi.org/10.1016/j.atmosenv.2010.07.019>
- Derwent, R. G., Jenkin, M. E., & Saunders, S. M. (1996). Photochemical ozone creation potentials for a large number of reactive hydrocarbons under European conditions. *Atmospheric Environment*, 30(2), 181–199. [https://doi.org/10.1016/1352-2310\(95\)00303-G](https://doi.org/10.1016/1352-2310(95)00303-G)
- Dickerson, R. R., Li, C., Li, Z., Marufu, L. T., Stehr, J. W., McClure, B., et al. (2007). Aircraft observations of dust and pollutants over northeast China : Insight into the meteorological mechanisms of transport. *Journal of Geophysical Research*, 112(x), 1–13. <https://doi.org/10.1029/2007JD008999>

- Ding, A. J., Wang, T., Thouret, V., Cammas, J.-P., & Nédélec, P. (2008). Tropospheric ozone climatology over Beijing: analysis of aircraft data from the MOZAIC program. *Atmospheric Chemistry and Physics*, 8(1), 1–13. <https://doi.org/10.5194/acp-8-1-2008>
- Environmental Protection Agency. (1999). *Compendium of Methods for the Determination of Toxic Organic Compounds in Ambient Air Second Edition Compendium Method TO-15 Determination Of Volatile Organic Compounds (VOCs) In Air Collected In Specially-Prepared Canisters And Analyzed By Gas Chromato.* Cincinnati, OH.
- Environmental Protection Agency - Integrated Risk Information System. (2003). *Integrated Risk Information System (IRIS) Chemical Assessment Summary: Benzene ; CASRN 71-43-2.*
- Finlayson-Pitts, B. J., & Pitts, J. N. (1999). *Chemistry of the Upper and Lower Atmosphere.* San Diego, CA: Academic Press.
- Fuchs, H., Tan, Z., Lu, K., Bohn, B., Broch, S., Brown, S. S., et al. (2017). OH reactivity at a rural site (Wangdu) in the North China Plain: Contributions from OH reactants and experimental OH budget. *Atmospheric Chemistry and Physics*, 17(1), 645–661. <https://doi.org/10.5194/acp-17-645-2017>
- Gao, B., Ju, X., Su, F., Meng, Q., Oenema, O., Christie, P., et al. (2014). Nitrous oxide and methane emissions from optimized and alternative cereal cropping systems on the North China Plain: A two-year field study. *Science of the Total Environment*, 472, 112–124. <https://doi.org/10.1016/j.scitotenv.2013.11.003>
- Geng, F., Zhang, Q., Tie, X., Huang, M., Ma, X., & Deng, Z. (2009). Aircraft measurements of O₃, NO_x, CO, VOCs, and SO₂ in the Yangtze River Delta region. *Atmospheric Environment*, 43(3), 584–593. <https://doi.org/10.1016/j.atmosenv.2008.10.021>
- Gilman, J. B., Kuster, W. C., Goldan, P. D., Herndon, S. C., Zahniser, M. S., Tucker, S. C., et al. (2009). Measurements of volatile organic compounds during the 2006 TexAQS/GoMACCS campaign: Industrial influences, regional characteristics, and diurnal dependencies of the OH reactivity. *Journal of Geophysical Research Atmospheres*, 114(7), 1–17. <https://doi.org/10.1029/2008JD011525>
- Gu, Y., Li, Q., Wei, D., Gao, L., Tan, L., Su, G., et al. (2019). Emission characteristics of 99 NMVOCs in different seasonal days and the relationship with air quality parameters in Beijing, China. *Ecotoxicology and Environmental Safety*, 169(September 2018), 797–806. <https://doi.org/10.1016/j.ecoenv.2018.11.091>
- Guenther, A. B., Zimmerman, P. R., Harley, P. C., & Monson, R. K. (1993). Isoprene and Monoterpene Emission Rate Variability' Model Evaluations and Sensitivity Analyses. *Journal of Geophysical Research*, 98617(20), 609–12. <https://doi.org/10.1029/93JD00527>
- Halliday, H. S., Thompson, A. M., Kollonige, D. W., & Martins, D. K. (2015). Reactivity and temporal variability of volatile organic compounds in the Baltimore / DC region in July 2011. *J Atmos Chem*, 72(July 2011), 197–213.

<https://doi.org/10.1007/s10874-015-9306-4>

- Halliday, H. S., Thompson, A. M., Wisthaler, A., Blake, D. R., Hornbrook, R. S., Mikoviny, T., et al. (2016). Atmospheric benzene observations from oil and gas production in the Denver-Julesburg Basin in July and August 2014. *Journal of Geophysical Research*, *121*(18), 11,055–11,074. <https://doi.org/10.1002/2016JD025327>
- He, H., Li, C., Loughner, C. P., Li, Z., Krotkov, N. A., Yang, K., et al. (2012). SO₂ over central China : Measurements , numerical simulations and the tropospheric sulfur budget. *Journal of Geophysical Research*, *117*, 1–15. <https://doi.org/10.1029/2011JD016473>
- He, H., Ren, X., Benish, S. E., Li, Z., Wang, F., Wang, Y., et al. (2019). Evaluation of Anthropogenic Emissions and Ozone Pollution in the North China Plain: Insights from the Air Chemistry Research in Asia (ARIAs) Campaign. *Atmos. Chem. Phys. Discuss, Under review*(March), 1–45.
- Helmig, D., & Bottenheim, J. (2009). Volatile organic compounds in the global atmosphere. *Eos, Transactions, American Geophysical Union*, *90*(52), 1–3. <https://doi.org/10.1029/2009EO520001>
- Huang, M., Crawford, J. H., Diskin, G. S., & Santanello, J. A. (2018). Modeling Regional Pollution Transport Events During KORUS-AQ : Progress and Challenges in Improving Representation of Land-Atmosphere Feedbacks. *Journal of Geophysical Research Atmospheres*, 732–756. <https://doi.org/10.1029/2018JD028554>
- Jerrett, M., Burnett, R. T., Pope, C. A., Ito, K., Thurston, G., Krewski, D., et al. (2009). Long-Term Ozone Exposure and Mortality. *New England Journal of Medicine*, *360*(11), 1085–1095. <https://doi.org/10.1056/NEJMoa0803894>
- Jia, C., Mao, X., Huang, T., Liang, X., Wang, Y., Shen, Y., et al. (2016). Non-methane hydrocarbons (NMHCs) and their contribution to ozone formation potential in a petrochemical industrialized city, Northwest China. *Atmospheric Research*, *169*, 225–236. <https://doi.org/10.1016/j.atmosres.2015.10.006>
- Johnson, D., Utembe, S. R., & Jenkin, M. E. (2006). Simulating the detailed chemical composition of secondary organic aerosol formed on a regional scale during the TORCH 2003 campaign in the southern UK. *Atmospheric Chemistry and Physics*, *6*(2), 419–431. <https://doi.org/10.5194/acp-6-419-2006>
- Kim, S., Sanchez, D., Wang, M., Seco, R., Jeong, D., Hughes, S., et al. (2016). OH reactivity in urban and suburban regions in Seoul, South Korea—an East Asian megacity in a rapid transition. *Faraday Discussions*, *189*, 231–251. <https://doi.org/10.1039/c5fd00230c>
- Kleinman, L. (2005a). A comparative study of ozone production in five U.S. metropolitan areas. *Journal of Geophysical Research*, *110*(D2), D02301. <https://doi.org/10.1029/2004JD005096>
- Kleinman, L. (2005b). The dependence of tropospheric ozone production rate on ozone precursors. *Atmospheric Environment*, *39*(3), 575–586. <https://doi.org/10.1016/j.atmosenv.2004.08.047>

- Klimont, Z., Streets, D. G., Gupta, S., Cofala, J., Lixin, F., & Ichikawa, Y. (2002). Anthropogenic emissions of non-methane volatile organic compounds in China. *Atmospheric Environment*, 36(8), 1309–1322. [https://doi.org/10.1016/S1352-2310\(01\)00529-5](https://doi.org/10.1016/S1352-2310(01)00529-5)
- Krotkov, N. A., McLinden, C. A., Li, C., Lamsal, L. N., Celarier, E. A., Marchenko, S. V., et al. (2016). Aura OMI observations of regional SO₂ and NO₂ pollution changes from 2005 to 2015. *Atmospheric Chemistry and Physics*, 16(7), 4605–4629. <https://doi.org/10.5194/acp-16-4605-2016>
- Lan, Q. (2004). Hematotoxicity in Workers Exposed to Low Levels of Benzene. *Science*, 306(5702), 1774–1776. <https://doi.org/10.1126/science.1102443>
- Lau, A. K. H., Yuan, Z., Yu, J. Z., & Louie, P. K. K. (2010). Source apportionment of ambient volatile organic compounds in Hong Kong. *Science of the Total Environment*, 408(19), 4138–4149. <https://doi.org/10.1016/j.scitotenv.2010.05.025>
- Li, C., Tsay, S. C., Fu, J. S., Dickerson, R. R., Ji, Q., Bell, S. W., et al. (2010). Anthropogenic air pollution observed near dust source regions in northwestern China during springtime 2008. *Journal of Geophysical Research*, 115, 1–18. <https://doi.org/10.1029/2009JD013659>
- Li, G., Bei, N., Cao, J., Wu, J., Long, X., Feng, T., et al. (2017). Widespread and persistent ozone pollution in eastern China during the non-winter season of 2015: Observations and source attributions. *Atmospheric Chemistry and Physics*, 17(4), 2759–2774. <https://doi.org/10.5194/acp-17-2759-2017>
- Li, L., Xie, S., Zeng, L., Wu, R., & Li, J. (2015). Characteristics of volatile organic compounds and their role in ground-level ozone formation in the Beijing-Tianjin-Hebei region, China. *Atmospheric Environment*, 113, 247–254. <https://doi.org/10.1016/j.atmosenv.2015.05.021>
- Liang, X., Chen, X., Zhang, J., Shi, T., Sun, X., Fan, L., et al. (2017). Reactivity-based industrial volatile organic compounds emission inventory and its implications for ozone control strategies in China. *Atmospheric Environment*, 162(2), 115–126. <https://doi.org/10.1016/j.atmosenv.2017.04.036>
- Lindaas, J., Farmer, D. K., Pollack, I. B., Abeleira, A., Flocke, F., Roscioli, R., et al. (2017). Changes in ozone and precursors during two aged wildfire smoke events in the Colorado Front Range in summer 2015. *Atmospheric Chemistry and Physics*, 17(17), 10691–10707. <https://doi.org/10.5194/acp-17-10691-2017>
- Liu, J., & Si, W. (2011). Using NDVI and air temperature to monitoring winter-wheat phenology in Xingtai, Hebei, China. *2011 International Conference on Control, Automation and Systems Engineering, CASE 2011*. <https://doi.org/10.1109/ICCASE.2011.5997798>
- Liu, Y., Shao, M., Fu, L., Lu, S., Zeng, L., & Tang, D. (2008). Source profiles of volatile organic compounds (VOCs) measured in China: Part I. *Atmospheric Environment*, 42(25), 6247–6260. <https://doi.org/10.1016/j.atmosenv.2008.01.070>
- Liu, Y., Shao, M., Kuster, W. C., Lu, S., & Gouw, J. A. D. E. (2009). Source Identification of Reactive Hydrocarbons and Oxygenated VOCs in the Summertime

- in Beijing. *Environmental Science & Technology*, 43(1), 75–81.
- Long, X., Tie, X., Cao, J., Huang, R., Feng, T., Li, N., et al. (2016). Impact of crop field burning and mountains on heavy haze in the North China Plain: A case study. *Atmospheric Chemistry and Physics*, 16(15), 9675–9691. <https://doi.org/10.5194/acp-16-9675-2016>
- Lu, X., Hong, J., Zhang, L., Cooper, O. R., Schultz, M. G., Xu, X., et al. (2018). Severe Surface Ozone Pollution in China: A Global Perspective. *Environmental Science and Technology Letters*. <https://doi.org/10.1021/acs.estlett.8b00366>
- Mazuca, G. M., Ren, X., Loughner, C. P., Estes, M., Crawford, J. H., Pickering, K. E., et al. (2016). Ozone production and its sensitivity to NO_x and VOCs: Results from the DISCOVER-AQ field experiment, Houston 2013. *Atmospheric Chemistry and Physics*, 16(22), 14463–14474. <https://doi.org/10.5194/acp-16-14463-2016>
- McDuffie, E. E., Edwards, P. M., Gilman, J. B., Lerner, B. M., Dubé, W. P., Trainer, M., et al. (2016). Influence of oil and gas emissions on summertime ozone in the Colorado Northern Front Range. *Journal of Geophysical Research*, 121(14), 8712–8729. <https://doi.org/10.1002/2016JD025265>
- Mellouki, A., Wallington, T. J., & Chen, J. (2015). Atmospheric Chemistry of Oxygenated Volatile Organic Compounds: Impacts on Air Quality and Climate. *Chemical Reviews*, 115(10), 3984–4014. <https://doi.org/10.1021/cr500549n>
- Mo, Z., Shao, M., Lu, S., Qu, H., Zhou, M., Sun, J., & Gou, B. (2015). Process-specific emission characteristics of volatile organic compounds (VOCs) from petrochemical facilities in the Yangtze River Delta, China. *Science of the Total Environment*, 533, 422–431. <https://doi.org/10.1016/j.scitotenv.2015.06.089>
- Moreira Dos Santos, C. Y., De Almeida Azevedo, D., & De Aquino Neto, F. R. (2004). Atmospheric distribution of organic compounds from urban areas near a coal-fired power station. *Atmospheric Environment*, 38(9), 1247–1257. <https://doi.org/10.1016/j.atmosenv.2003.11.026>
- Na, K., Kim, Y. P., Moon, K., Moon, I., & Fung, K. (2001). Concentrations of volatile organic compounds in an industrial area of Korea. *Atmospheric Environment*, 35.
- Okada, Y., & Nakagoshi, A. (2012). Environmental risk assessment and concentration trend of atmospheric volatile organic compounds in Hyogo. *Environmental Science Pollution Research*, 201–213. <https://doi.org/10.1007/s11356-011-0550-0>
- Perry, R., & Gee, I. L. (1995). Vehicle emissions in relation to fuel composition. *Science of the Total Environment*, 169(1–3), 149–156. [https://doi.org/10.1016/0048-9697\(95\)04643-F](https://doi.org/10.1016/0048-9697(95)04643-F)
- Pfister, G., Flocke, F., Hornbrook, R., Orlando, J., & Lee, S. (2017). *Process-Based and Regional Source Impact Analysis for FRAPPÉ and DISCOVER-AQ 2014* (Vol. 2016000120). Retrieved from https://www.colorado.gov/airquality/tech_doc_repository.aspx?action=open&file=FRAPPE-NCAR_Final_Report_July2017.pdf
- Ran, L., Zhao, C. S., Xu, W. Y., Lu, X. Q., Han, M., Lin, W. L., et al. (2011). VOC

- reactivity and its effect on ozone production during the HaChi summer campaign. *Atmospheric Chemistry and Physics*, 11(10), 4657–4667. <https://doi.org/10.5194/acp-11-4657-2011>
- Reich, P. B., & Amundson, R. G. (1985). Ambient levels of ozone reduce net photosynthesis in tree and crop species. *Science*, 230(4725), 566–570. <https://doi.org/10.1126/science.230.4725.566>
- Ren, X., Salmon, O. E., Hansford, J. R., Ahn, D., Hall, D., Benish, S. E., et al. (2018). Methane Emissions from the Baltimore-Washington Area Based on Airborne Observations: Comparison to Emissions Inventories. *Journal of Geophysical Research: Atmospheres*, 1–14. <https://doi.org/10.1029/2018JD028851>
- Ryerson, T. B., Trainer, M., Angevine, M., Brock, C. A., Dissly, R. W., Fehsenfeld, F. C., et al. (2003). Effect of petrochemical industrial emissions of reactive alkenes and NO_x on tropospheric ozone formation in Houston, Texas. *Journal of Geophysical Research*, 108(D8), 4249. <https://doi.org/10.1029/2002JD003070>
- Sadanaga, Y., Yoshino, A., Kato, S., & Kajii, Y. (2005). Measurements of OH reactivity and photochemical ozone production in the urban atmosphere. *Environmental Science and Technology*, 39(22), 8847–8852. <https://doi.org/10.1021/es049457p>
- Saunders, S. M., Jenkin, M. E., Derwent, R. G., & Pilling, M. J. (2003). Protocol for the development of the Master Chemical Mechanism, MCM v3 (Part A): Tropospheric degradation of non-aromatic volatile organic compounds. *Atmospheric Chemistry and Physics*, 3(1), 161–180. <https://doi.org/10.5194/acp-3-161-2003>
- Seiber, J. N. (1996). TOXIC AIR CONTAMINANTS IN URBAN ATMOSPHERES : EXPERIENCE IN CALIFORNIA. *Atmospheric Environment*, 30(5), 751–756.
- Shao, M., Zhang, Y., Zeng, L., Tang, X., Zhang, J., Zhong, L., & Wang, B. (2009). Ground-level ozone in the Pearl River Delta and the roles of VOC and NO_x in its production. *Journal of Environmental Management*. <https://doi.org/10.1016/j.jenvman.2007.12.008>
- Sillman, S., Logan, A., & Wofsy, C. (1990). The Sensitivity of Ozone to Nitrogen Oxides and Hydrocarbons in Regional Ozone Episodes 1 Now at of Atmospheric , Oceanic , and Space Sciences , al ., to explore the factors that influence ozone in Michigan , al areas during stagnation periods , again foc. *Journal of Geophysical Research*, 95, 1837–1851.
- Simpson, I. J., Colman, J. J., Swanson, A. L., & Bandy, A. R. (2001). Aircraft Measurements of Dimethyl Sulfide (DMS) Using a Whole Air Sampling Technique. *Journal of Atmospheric Chemistry*, 191–213.
- Simpson, I. J., Blake, N. J., Blake, D. R., Atlas, E., Flocke, F., Crawford, J. H., et al. (2003). Photochemical production and evolution of selected C₂ – C₅ alkyl nitrates in tropospheric air influenced by Asian outflow. *Journal of Geophysical Research*, 108. <https://doi.org/10.1029/2002JD002830>
- Simpson, I. J., Blake, N. J., Barletta, B., Diskin, G. S., Fuelberg, H. E., Gorham, K., et al. (2010). Characterization of trace gases measured over Alberta oil sands mining operations: 76 speciated C₂–C₁₀ volatile organic compounds. *Atmos. Chem. Phys.*

11931–11954. <https://doi.org/10.5194/acp-10-11931-2010>

- Simpson, I. J., Akagi, S. K., Barletta, B., Blake, N. J., Choi, Y., Diskin, G. S., et al. (2011). Boreal forest fire emissions in fresh Canadian smoke plumes : C1C10 volatile organic compounds (VOCs), CO₂, CO, NO₂, NO, HCN and Ch₃CN. *Atmospheric Chemistry and Physics*, 6445–6463. <https://doi.org/10.5194/acp-11-6445-2011>
- Stavrakou, T., Müller, J., Bauwens, M., Smedt, I. De, Lerot, C., & Roozendaal, M. Van. (2016). Substantial Underestimation of Post-Harvest Burning Emissions in the North China Plain Revealed by Multi-Species Space Observations. *Nature Publishing Group*, (August), 1–11. <https://doi.org/10.1038/srep32307>
- Stroud, C. A., Morneau, G., Makar, P. A., Moran, M. D., Gong, W., Pabla, B., et al. (2008). OH-reactivity of volatile organic compounds at urban and rural sites across Canada: Evaluation of air quality model predictions using speciated VOC measurements. *Atmospheric Environment*, 42(33), 7746–7756. <https://doi.org/10.1016/j.atmosenv.2008.05.054>
- Tang, G., Wang, Y., Li, X., Ji, D., Hsu, S., & Gao, X. (2012). Spatial-temporal variations in surface ozone in Northern China as observed during 2009–2010 and possible implications for future air quality control strategies. *Atmospheric Chemistry and Physics*, 12(5), 2757–2776. <https://doi.org/10.5194/acp-12-2757-2012>
- Tang, J. H., Chan, L. Y., Chan, C. Y., Li, Y. S., Chang, C. C., Liu, S. C., et al. (2007). Characteristics and diurnal variations of NMHCs at urban, suburban, and rural sites in the Pearl River Delta and a remote site in South China. *Atmospheric Environment*, 41(38), 8620–8632. <https://doi.org/10.1016/j.atmosenv.2007.07.029>
- Tang, J. H., Chan, L. Y., Chang, C. C., Liu, S., & Li, Y. S. (2009). Characteristics and sources of non-methane hydrocarbons in background atmospheres of eastern, southwestern, and southern China. *Journal of Geophysical Research Atmospheres*, 114(3). <https://doi.org/10.1029/2008JD010333>
- Tsai, C., Chen, M., Chang, K., Chang, F., & Mao, I. (2009). The pollution characteristics of odor , volatile organochlorinated compounds and polycyclic aromatic hydrocarbons emitted from plastic waste recycling plants. *Chemosphere*, 74(8), 1104–1110. <https://doi.org/10.1016/j.chemosphere.2008.10.041>
- Wang, B., Shao, M., Lu, S. H., Yuan, B., Zhao, Y., Wang, M., et al. (2010). Variation of ambient non-methane hydrocarbons in Beijing city in summer 2008. *Atmos. Chem. Phys*, 5911–5923. <https://doi.org/10.5194/acp-10-5911-2010>
- Wang, F., Li, Z., Ren, X., Jiang, Q., He, H., Dickerson, R. R., et al. (2018). Vertical distributions of aerosol optical properties during the spring 2016 ARIAs airborne campaign in the North China Plain. *Atmospheric Chemistry and Physics Discussions*, (January), 1–22. <https://doi.org/10.5194/acp-2017-1021>
- Wang, G., Cheng, S., Wei, W., Zhou, Y., Yao, S., & Zhang, H. (2016). Characteristics and source apportionment of VOCs in the suburban area of Beijing , China. *Atmospheric Pollution Research*, 7(4), 711–724. <https://doi.org/10.1016/j.apr.2016.03.006>

- Wang, H., Qiao, Y., Chen, C., Lu, J., Dai, H., Qiao, L., et al. (2014). Source profiles and chemical reactivity of volatile organic compounds from solvent use in Shanghai, China. *Aerosol and Air Quality Research*, *14*(1), 301–310. <https://doi.org/10.4209/aaqr.2013.03.0064>
- Wang, H. L., Nie, L., Li, J., Wang, Y. F., Wang, G., Wang, J. H., & Hao, Z. P. (2012). Characterization and assessment of volatile organic compounds (VOCs) emissions from typical industries. *Chinese Science Bulletin*, *58*(7), 724–730. <https://doi.org/10.1007/s11434-012-5345-2>
- Wang, Y., Li, Z., Zhang, Y., Du, W., Zhang, F., Tan, H., et al. (2018). Characterization of aerosol hygroscopicity, mixing state, and CCN activity at a suburban site in the central North China Plain. *Atmospheric Chemistry and Physics Discussions*, 1–34. <https://doi.org/10.5194/acp-2017-1100>
- Wang, Y., Dorner, S., Donner, S., Beirle, S., Wang, Y., Dong, Z., et al. (2018). Vertical profiles and sources of NO₂, SO₂, HONO, HCHO, CHOCHO, and aerosols derived from MAX-DOAS measurements at a rural site in the central-western North China Plain. *Atmos. Chem. Phys.*
- Wei, W., Wang, S., Chatani, S., Klimont, Z., Cofala, J., & Hao, J. (2008). Emission and speciation of non-methane volatile organic compounds from anthropogenic sources in China. *Atmospheric Environment*, *42*(20), 4976–4988. <https://doi.org/10.1016/j.atmosenv.2008.02.044>
- Wolfe, G. M., Marvin, M. R., Roberts, S. J., Travis, K. R., & Liao, J. (2016). The framework for 0-D atmospheric modeling (F0AM) v3.1. *Geoscientific Model Development*, *9*(9), 3309–3319. <https://doi.org/10.5194/gmd-9-3309-2016>
- Wu, R., Bo, Y., Li, J., Li, L., Li, Y., & Xie, S. (2016). Method to establish the emission inventory of anthropogenic volatile organic compounds in China and its application in the period 2008–2012. *Atmospheric Environment*, *127*, 244–254. <https://doi.org/10.1016/j.atmosenv.2015.12.015>
- Wu, W., Zhao, B., Wang, S., & Hao, J. (2017). Ozone and secondary organic aerosol formation potential from anthropogenic volatile organic compounds emissions in China. *Journal of Environmental Sciences (China)*, *53*, 224–237. <https://doi.org/10.1016/j.jes.2016.03.025>
- Xie, X., Shao, M., Liu, Y., Lu, S., Chang, C. C., & Chen, Z. M. (2008). Estimate of initial isoprene contribution to ozone formation potential in Beijing, China. *Atmospheric Environment*, *42*(24), 6000–6010. <https://doi.org/10.1016/j.atmosenv.2008.03.035>
- Xue, L. K., Wang, T., Gao, J., Ding, a. J., Zhou, X. H., Blake, D. R., et al. (2013). Ozone production in four major cities of China: sensitivity to ozone precursors and heterogeneous processes. *Atmospheric Chemistry and Physics Discussions*, *13*(10), 27243–27285. <https://doi.org/10.5194/acpd-13-27243-2013>
- Yang, X., Wang, X., Yang, W., Xu, J., Ren, L., He, Y., et al. (2016). Aircraft measurements of SO₂, NO_x, CO, and O₃ over the coastal and offshore area of Yellow Sea of China. *Environmental Monitoring and Assessment*, *188*(9). <https://doi.org/10.1007/s10661-016-5533-7>

- Yang, Y., Shao, M., Keßel, S., Li, Y., Lu, K., Lu, S., et al. (2016). How does the OH reactivity affect the ozone production efficiency: case studies in Beijing and Heshan. *Atmospheric Chemistry and Physics Discussions*, *0*, 1–37. <https://doi.org/10.5194/acp-2016-507>
- Yuan, B., Hu, W. W., Shao, M., Wang, M., Chen, W. T., Lu, S. H., et al. (2013). VOC emissions, evolutions and contributions to SOA formation at a receptor site in eastern China. *Atmospheric Chemistry and Physics*, *13*(17), 8815–8832. <https://doi.org/10.5194/acp-13-8815-2013>
- Zhang, F., Zhou, L. X., Novelli, P. C., Worthy, D. E. J., Zellweger, C., Klausen, J., et al. (2011). Evaluation of in situ measurements of atmospheric carbon monoxide at Mount Waliguan, China. *Atmospheric Chemistry and Physics*, *11*(11), 5195–5206. <https://doi.org/10.5194/acp-11-5195-2011>
- Zhang, Q., Streets, D. G., Carmichael, G. R., He, K. B., Huo, H., Kannari, A., et al. (2009). Asian emissions in 2006 for the NASA INTEX-B mission. *Atmospheric Chemistry and Physics*, *9*(14), 5131–5153. <https://doi.org/10.5194/acp-9-5131-2009>
- Zhang, Q., Yuan, B., Shao, M., Wang, X., Lu, S., Lu, K., et al. (2014). Variations of ground-level O₃ and its precursors in Beijing in summertime between 2005 and 2011. *Atmospheric Chemistry and Physics*, *14*(12), 6089–6101. <https://doi.org/10.5194/acp-14-6089-2014>
- Zhang, Y., Li, C., Wang, X., Guo, H., Feng, Y., & Chen, J. (2012). Rush-hour aromatics and chlorinated hydrocarbons in selected subway stations of Shanghai, China. *Journal of Environmental Sciences*, *24*(1), 131–141. [https://doi.org/10.1016/S1001-0742\(11\)60736-5](https://doi.org/10.1016/S1001-0742(11)60736-5)
- Zheng, J., Shao, M., Che, W., Zhang, L., Zhong, L., Zhang, Y., & Streets, D. (2009). Speciated VOC Emission Inventory and Spatial Patterns of Ozone Formation Potential in the Pearl River Delta, China. *Environmental Science and Technology*, *43*(22), 8580–8586.